PAN-SHARPENING THE SPATIAL RESOLUTION OF MULTISPECTRAL IMAGE FOR THE ASSESSMENT OF NEAR-SHORE BATHYMETRY

Thesis

Submitted in partial fulfillment of the requirements for the degree of

DOCTOR OF PHILOSOPHY

by

JAGALINGAM P

DEPARTMENT OF APPLIED MECHANICS AND HYDRAULICS

NATIONAL INSTITUTE OF TECHNOLOGY KARNATAKA

SURATHKAL, MANGALURU - 575025

January, 2018

PAN-SHARPENING THE SPATIAL RESOLUTION OF MULTISPECTRAL IMAGE FOR THE ASSESSMENT OF NEAR-SHORE BATHYMETRY

Thesis

Submitted in partial fulfillment of the requirements for the degree of

DOCTOR OF PHILOSOPHY

by

JAGALINGAM P

Under the guidance of

DR. ARKAL VITTAL HEGDE

Professor

Dept. of Applied Mechanics & Hydraulics

NITK Surathkal

DEPARTMENT OF APPLIED MECHANICS & HYDRAULICS

NATIONAL INSTITUTE OF TECHNOLOGY KARNATAKA

SURATHKAL, MANGALURU - 575025

January, 2018

DEDICATION

Every challenging work needs self effort as well as guidance of elders especially those who were very close to our heart.

My humble effort I dedicate to my sweet and loving

Father and Mother

My special dedication to my better-half and lovely

wife

Whose affection, love, encouragement and prays of day and night make me able to get such success and honour,

Along with all hard working and respected *Teachers*

DECLARATION

By the Ph.D. Research Scholar

I hereby *declare* that the Research Thesis entitled **PAN-SHARPENING THE SPATIAL RESOLUTION OF MULTISPECTRAL IMAGE FOR THE ASSESSMENT OF NEAR-SHORE BATHYMETRY** which is being submitted to the **National Institute of Technology Karnataka, Surathkal** in partial fulfillment of the requirements for the award of the Degree of **Doctor of Philosophy** in **Remote sensing** is a *bonafide report of the research work carried out by me*. The material contained in this Research Thesis has not been submitted to any University or Institution for the award of any degree.

JAGALINGAM P

Reg. No.: 138031 AM13F05

DEPARTMENT OF APPLIED MECHANICS AND HYDRAULICS

Place: NITK, Surathkal.

Date: January 10, 2018

CERTIFICATE

This is to *certify* that the Research Thesis entitled **PAN-SHARPENING THE SPATIAL RESOLUTION OF MULTISPECTRAL IMAGE FOR THE ASSESSMENT OF NEAR-SHORE BATHYMETRY** submitted by **JAGALINGAM P**, (Reg. No.: 138031 AM13F05) as the record of the research work carried out by him, is *accepted as the Research Thesis submission* in partial fulfillment of the requirements for the award of degree of **Doctor of Philosophy**.

(Prof. Arkal Vittal Hegde)
Research Supervisor

Chairman - DRPC

ACKNOWLEDGMENT

I feel it is a great privilege to express my deepest and most sincere gratitude to my supervisor, Prof. Arkal Vittal Hegde for his suggestions, constant encouragement and support during the course of the work. With deepest gratitude, I like to express sincere thanks to my supervisor for guidance, backgroud knowledge, patience and editing skills in the completion of this document. Many of the ideas in the thesis originally came from my discussions with the professor. I have whole heartedly enjoyed the challenge of examining and researching a prominent issue that could greatly impact society and public education instead of just performing another educational study. I am also grateful to the other members of my doctoral committee, namely Prof. A. O. Surendranathan and Dr. Manu for their valuable comments on my work. I take this opportunity to thank Prof. Subba Rao and Prof. G. S. Dwarkish, the former head and the present Head of Department of Applied Mechanics and Hydraulics for their kindness and continuous support. I would like to extend my deepset gratitude towards all the other faculty members of the department for their never-ending support, encouragement and help.

I extend my sincere thanks to Mr. Jagadish, Mr. Balakrishna and all other non-teaching satff for their extended support and unrelenting efforts in structuring this research. I thank all my fellow research scholars and M.Tech students for their cooperation. My thanks also go out to all my friends who have rendered their help at different times which made my stay in this institute a memorable period of my life.

Finally, special recognition goes out to my parents, wife, brother, sister and family for their unbounded love, encouragement and patience during my pursuit of Doctorate in Applied Mechanics and Hydraulics Engineering. I am deeply indebted to them for their countless sacrifices and support without which my research work would not have finished.

Place: NITK, Surathkal Jagalingam P

Date: January 10, 2018

ABSTRACT

A numerous earth observing satellites have been launched to the orbit to capture the images of the earth surface. The satellite acquires images of earth surface in panchromatic (Pan) and multispectral (MS) modes. The Pan image contains high spatial details whereas MS image holds rich spectral information but low spatial resolution. The remote sensing applications require both the qualities in a single image.

Many pan-sharpening methods were developed to transfer the spatial detail of Pan image to the MS image, to have a single image with both high spatial and rich spectral information. One of the primary objectives of the present research is to determine the suitable pan-sharpening technique for improving the spatial resolution and retaining the spectral information of MS image. Therefore, the present study focuses on nine different pan-sharpening methods like principal component analysis (PCA), modified-intensity hue saturation (M-IHS), multiplicative, brovey transform (BT), wavelet principal component analysis (W-PCA), hyperspherical colour sharpening (HCS), high pass filter (HPF), gram-schmidt (GS) and Fuze Go. These were used for fusing the Pan and MS imageries of Quickbird-2 and Landsat-8. The effectiveness of these pan-sharpening method should not distort the spectral information of an MS image while enhancing the spatial resolution.

To evaluate the performance of the above mentioned pan-sharpening methods, both qualitative and quantitative approaches were adopted. In the quantitative approach the spectral indices like correlation coefficient (CC), structural similarity index measure (SSIM), root mean square error (RMSE), signal to noise ratio (SNR), universal quality index (Q) and peak signal noise ratio (PSNR) were used to assess the spectral quality of pan-sharpened image. The spatial indices like correlation coefficient (SCC), Gradient and image entropy (E) were used to assess the spatial quality of pan-sharpened image. Further, quality with no reference (QNR) indices were also performed to evaluate both spectral and spatial quality of pan-sharpened image. The results of qualitative and quantitative approaches indicate that the Fuse Go method outperformed other

pan-sharpening methods in providing a image with the highest spatial details and rich spectral information.

In addition, the effectiveness of improving the spatial resolution of MS image was studied by employing the Fuse Go pan-sharpened image for the extraction of buildings using Quickbird-2 imagery and for estimating the bathymetry of near shore ocean using Landsat-8 imagery.

To extract the buildings from the original and Fuze Go pan-sharpened Quickbird-2 imagery, both automatic and manual approaches were adopted and compared using qualitative and metric analysis. In automatic approach firstly, the vegetation portion were removed from the input image. Secondly, adaptive k-means clustering algorithm were adopted to cluster the pixels into different classes. Finally, the morphological fill and open operator was implemented to extract the buildings. In the manual approach, area of interest (AOI) was created from the input image. Later, the generated AOI was used to subset the interested features from the image. The results of qualitative and metric analysis indicate that the building detection percentage of automatic algorithm for the original and pan-sharpened image are reasonable for such a challenging MS image. The results of manual method indicate that the extraction of buildings is achieved with minimum loss of information in comparison with the automatic method. However, improving the spatial resolution of the original MS image, helps to determine the buildings information more precisely in terms of spatially as well as spectrally.

The procedure based on ratio-transform algorithm was adopted on original and Fuse Go pan-sharpened imagery of Landsat-8 for estimating the bathymtery of near shore ocean along the coast of Mangaluru, India. The performance of the procedure was evaluated using root mean square error (RMSE) and mean absolute error (MAE). The results of RMSE and MAE indicate that the procedure better estimates the depth up to 5 m and 10 m for the original and improved spatial resolution of Landsat-8 imagery. Therefore, the Fuse Go method can be used for remote sensing applications, which demands both high spatial and spectral information in a single image.

Keywords: Pan-sharpening, Spatial, Spectral, Qualitative, Quantitative, Adaptive K-means algorithm, Morphological operators, Ratio transform algorithm

Contents

List of Figures

List of Tables

Acronyms and Abbreviations

Abbreviations	Description
Landsat	Land Remote-Sensing Satellite (System)
IRS	Indian Remote Sensing
SPOT	Satellite Pour observation de la Terre
Pan	Panchromatic
MS	Multispectral
PCA	Principal Component Analysis
IHS	Intensity Hue Saturation
M-IHS	Modified-Intensity Hue Saturation
BT	Brovey Transform
SRM	Subtractive Resolution Merge
HCS	Hypersherical Colour Sharpening
HPF	High Pass Filter
GS	Gram Schmidt
W-PCA	Wavelet Principal Component Analysis
W-IHS	Wavelet Intensity Hue Saturation
RMSE	Root Mean Square Error
SAM	Spectral Angular Mapper
ERGAS	Relative Dimensionless Global Error
MB	Mean Bias

Abbreviations	Description
PFE	Percentage Fit Error
SNR	Signal to Noise Ratio
PSNR	Peak Signal to Noise Ratio
CC	Correlation Coefficient
RASE	Relative Average Spectral Error
SSIM	Structural Similarity Index Measure
SCC	Spatial Correlation Coefficient
E	Image Entropy
SF	Spatial Frequency
QNR	Quality with No Reference
ALB	Airborne Laser Bathymetric
LiDAR	Light Detection and Ranging
SHOLAS	Scanning Hydrographic Operational Airborne Lidar Survey
CHARTS	Compact Hydrographic Airborne Rapid Total Survey
LADS	Laser Airborne Depth Sounder
EAARL	Experimental Advanced Airborne Research Lidar
DWT	Discrete Wavelet Transform
DT-CWT	Dual-Tree Complex Wavelet Transform
HPFA	High Pass Filter Additive
DFB	Directional Filter Bank
LRPISYN	Low Resolution Panchromatic Synthetic Image
HRPISYN	High Resolution Panchromatic Synthetic Image
HPF	High Pass Filter
LPF	Low Pass Filter

Abbreviations	Description
NSCT	Nonsubsampled Contourlet Transform
GIHS	Generalized Intensity Hue Saturation
WT	Wavelet Transform
MCA	Morphological Component Analysis
AIHS	Adaptive Intensity Hue Saturation
MRF	Markov Random Field
TM	Thematic Mapper
ETM	Enhanced Thematic Mapper
LULC	Land Use/Land Cover
RGB	Red Green Blue
NIR	Near Infrared
HSV	Hue Saturation Value
LISS	Linear Imaging Self Scanning Sensor
NMPT	New Mangalore Port Trust
Q	Universal Quality Index
GIS	Geographic Information System
DP	Detection percentage
BF	Branch Factor
TP	True Positive
FP	False Positive
TN	True Negative
AOI	Area of Interest
USGS	United States Geological Survey
MLLW	Mean Lower Low Water
LAT	Lowest Astronomical Tide

List of Symbols and Notations

Symbol	Explanation
(σ)	Standard deviation
R^2	Co-efficient of determination
x	Reference image
y	Pan-sharpened image
x_i	Mean of the reference image
y_i	Mean of the pan-sharpened image
n	Number of elements
L	Number of gray levels in the image
$x(i,j)$	Pixel value of the reference image
$y(i,j)$	Pixel value of the pan-sharpened image
f	Pan image
μ_f	Mean of the Pan image
$p(i)$	Pixel occurrence frequency of grayscale value i in the image
m,n	Grayscale level of the pixel
$\Delta xf(i,j)$, $\Delta yf(i,j)$	First-order difference of pixel (i,j) along the x and y directions
σ_x	Standard deviations of reference
σ_y	Standard deviations of pan-sharpened image
c_1, c_2	Constants

Symbol	Explanation
a	Original MS image
f_{lp}	Low-resolution Pan image at the scale of MS image
m_1, m_0	Gain and Offset
R_i	Pixel value in B and G band
b_i	Regression slope
Min_{NIR}	Minimum NIR Brightness
L_{obs}	Observed radiance of bands
i	Blue band
j	Green band
z	Depth in meter
r_i	Reference data
t_i	Algorithm result

Chapter 1

INTRODUCTION

1.1 General

The chapter provides the brief introduction of Remote sensing, Pan-sharpening, Extraction of buildings and Bathymetry mapping.

1.2 Remote sensing

Remote sensing is a significant tool for capturing the images of the earth surface. To obtain such images, many countries began to launch earth observing satellites such as LANDSAT, IRS, SPOT, and Quickbird series etc. All these satellites were launched to the orbit carrying two different sensors, one for capturing the image in Pan (black and white) band and the other for capturing the image in multiple bands. These satellite sensors record images of the land surface and send them to the ground stations. These images help researchers to visually interpret the features present on the earth surface and to analyse changes of various features over a certain period.

The former provides the Pan images in only a single band with high spatial resolution, whereas the latter can provide images in multiple bands with rich spectral resolution, but low spatial resolution (Zhang and Mishra, 2013). Pan images of high spatial resolution enable analysis and differentiation of the features based on spatial detail; MS images with high spectral resolution can differentiate the features based on spectral information (Ranchin and Wald, 2000). For every successive launch of the earth observing satellites into orbit, both Pan and MS sensors are upgraded to higher versions for capturing the images with improved spatial detail and rich spectral resolution. How-

ever, satellites launched into orbit till date have not been able to acquire images with both high spatial and rich spectral resolution in a single image (Nikolakopoulos, 2008), even though remote sensing applications such as feature extraction and classification demand a single image with both high spatial and rich spectral information (Ghosh and Joshi, 2013).

The sensors have two technical constraints for delivering an image with both high spatial and rich spectral resolution (Zhang, 2004). The first is the quantity of radiation energy received by the sensor. Traditionally, Pan sensors are designed to capture an image in a broader range of wavelengths, whereas MS sensors cover a much smaller range of wavelengths (Yusuf et al., 2012). The size of the Pan detector is smaller than that of the MS detector. Thus, the energy collected by Pan detectors over the broader range of wavelengths provides high spatial resolution but decreased the spectral resolution, whereas the energy collected by MS detectors over the narrow range of wavelengths provides high spectral resolution but decreased spatial resolution (Amro et al., 2011). The second constraint is the amount of information collected by the sensor. The amount of information collected by an MS sensor with the spatial resolution of a Pan sensor may lead to technical limitations in on-board storage capacity and the transmission rate of data from space to the ground station (Nikolakopoulos, 2008). The alternate solution for the limitation of sensor is an pan-sharpening or image fusion techniques.

1.3 Pan-sharpening

Pan-sharpening is the process of fusing the high spatial details of a Pan image and the rich spectral resolution of an MS image by transferring the spatial information of the Pan image to the MS image while retaining the spectral data of the MS image to create a single image with both high spatial and rich spectral information (Zhang, 2010). From late 1980 to present, many pan-sharpening techniques have been developed such as PCA (Chavez and Kwarteng, 1989), M-IHS (Siddiqui, 2003), multiplicaptive (Crippen, 1989), BT (Hallada and Cox, 1983), SRM (Ashraf et al., 2012), Ehlers (Ehlers et al., 1984), HCS (Padwick et al., 2010), HPF (Chavez et al., 1991), GS (Laben and Brower, 2000) and some hydrid fusion methods such as W-PCA and W-IHS. These hy-

brid methods work by the principle of wavelet decomposition (King and Wang, 2001). Further detail work of this method can be found in (Gonzalez-Audicana et al., 2005).

During the process of pan-sharpening, the two most key quality aspects of fused images are the enhancement of spatial resolution and preservation of spectral information. In other words, the effectiveness of image pan-sharpening algorithm should not distort the spectral information of an MS image while enhancing the spatial resolution. To evaluate the performance of the pan-sharpening methods, researchers have proposed methods of qualitative (visual) and quantitative analyses. The visual analysis evaluates the quality of fused image by visual interpretation (Fonseca et al., 2011). The quantitative analysis is adopted using two approaches namely, i) with reference image and ii) without reference image. When the reference image is available, the following quality metrics like, RMSE (Zoran, 2009), SAM (Alparone et al., 2007), ERGAS (Du et al., 2007), MB (Yusuf et al., 2012), PFE (Naidu, 2010), SNR (Alimuddin et al., 2012), PSNR (Naidu, 2010; Kumar and Singh, 2010), CC (Vandermeer, 2006), RASE (Wald, 2000), SSIM (Wang et al., 2004), SCC (Choi, 2006), Gradient (Wu et al., 2015) and E (Du et al., 2007) may be used. The reference image, which is an important requirement for processing the above mentioned indices, should be an MS image with the same size as that of Pan image. When the reference image is not available, the quality of the fused image is evaluated using the following quality metrics, such as σ (Wang and Chang, 2011), SF (Yang et al., 2010) and QNR image (Alparone et al., 2008). More details of quantitative analysis can be found in (Shahdoosti and Ghassemian, 2015).

The effectiveness of improving the spatial resolution of MS image can be addressed using various remote sensing applications. However, in the present work, two applications have been taken up namely, i) Extraction of buildings, ii) Estimating the bathymetry of near-shore ocean.

1.4 Extraction of buildings

Extraction of buildings from remote sensing satellite imagery is one of the most challenging problems. Recently, improvement in the spatial and spectral resolution of remote sensing satellite imagery has driven researchers to develop different algorithms

(i.e. automatic and semi-automatic) for the extraction of buildings from very high resolution satellite imageries. Detection of buildings from the satellite imagery has various significant applications in the domain of urban mapping, urban planning, urban change detection analysis, target detection and GIS (Shorter and Kasparis, 2009). Further, detection of buildings is important to assess the extent of destruction caused after natural disasters such as floods, earthquake and military operation.

Many factors that appear in the satellite imageries, have made the extraction of buildings, more complex and difficult, even though the new sensors provide satellite imageries with improved resolutions. Factors such as scene complexity, building variability and sensor resolution (Mayer, 1999) affect the overall accuracy for the detection of buildings. The man-made feature (i.e. building) is one of the most significant features among the other features, which consumes time and cost to extract, for the reason of their variability, complexity and abundance in urban areas (Chaudhuri et al., 2016).

Generally, very high resolution satellite imagery is necessary to extract detailed spatial and spectral information of buildings. In reality, procurement of very high resolution satellite imagery is expensive. On the other hand, pan-sharpening or image fusion methods are developed to obtain the image with both high spatial and spectral resolution. Therefore, to meet this goal, various image fusion or pan-sharpening methods have been proposed in the literature to improve the spatial resolution of MS imageries.

1.5 Bathymetry mapping

Estimating the bathymetry of ocean is one of the important parameters which plays a significant role in planning near-shore structure activities like engineering work, port management, pipeline laying, fishing, dredging operation, oil drilling, aquaculture, etc., and it is also significantly important to determine the underwater topography, movement of sediments and to generate hydrographic charts for safe ocean transportation.

Typically, the depth of ocean is measured using conventional methods such as pre-measured rope or cable passage, placed on the side of the vessel and allowed to reach the seabed. This method can retrieve the depth of a single point in time. This method was soon replaced by echo-sounders fitted to hydrographic ships such as single beam and

multi beam echo-sounders. The echo-sounding method is capable of determining the depths accurately over clear water coastal environment, In the shallow water environment, the method is often inaccessible to the hydrographic ships carrying the sounding instruments (Su et al., 2014). Generally, the speed of ship constrains the surveyors to map the ocean region at a slightly different scale than the desired scale. It is to be noted that the method would take about 200 years of survey time to complete swath survey of deep ocean and it would take even more time for shallow coastal areas (Carron et al., 2001).

In order to overcome this inefficiency, various ALB and LiDAR systems like LADS, CHARTS, SHOLAS and EAARL etc., were established to infer the bathymetry of oceans. This method can effectively determine the depth of both shallow and clear water deep coastal environment, but this technique is limited by its high purchasing and maintenance costs.

Almost all of the above methods take a long interval of time to revisit the same location and thus it is difficult to monitor the frequent changes of seabed morphology. Further, it is difficult to infer the bathymetry of shallow water region, as those areas are inflexible to access by hydrographic ships carrying echo sounding instruments. Remote sensing technology can be regarded as one of the most promising alternative tools to map the bathymetry of shallow water regions by pairing remote sensing data with ground based measurements (Winterbottom and Gilvear, 1997).

Bathymetry mapping using remote sensing technology is attained from the principle in which the total amount of electromagnetic energy observed and reflected from the water body determines the water depth. The remote sensing technique is available to determine the depth of ocean, for the reason that the water attenuates signal from the bottom of the ocean with a strong wavelength dependency (Dekker et al., 2011). On the other hand, penetration of electromagnetic wave energy is limited. Therefore, remote sensing technique is primarily adopted to infer the depth of clear and shallow water region (Zheng et al., 2014).

The two important approaches such as analytical method and empirical method are adopted to retrieve the bathymetry of ocean using satellite image. A number of ana-

lytical algorithms are available in literature, which are proposed by (Lyzenga, 1981; Lyzenga et al., 2006; Philpot, 1989). In order to adopt the analytical method for mapping the bathymetry of ocean, a number of input parameters such as water column, properties of atmosphere and bottom reflectance, spectral signatures of suspended and dissolved materials etc., are required (Spitzer and Dirks, 1986). Though the analytical method is moderately complex and difficult, it has been adopted by many researchers (Mobley et al., 2005; Brando et al., 2009; Giardino et al., 2012). On the other hand, the empirical method establishes the relationship between the remotely observed light of water body and the depth of water at sampled locations and depth is determined empirically without regard to how light is diffused in water (Gao, 2009). By comparison, empirical method requires only a few parameters as input and does not require water column parameters. However, for the calibration function, the method requires hydrographically measured data.

A number of empirical algorithms have been proposed to retrieve the bathymetry of ocean, among which the most commonly used algorithm is the ratio transform algorithm developed by (Stumpf et al., 2003). The ratio transform algorithm operates by the mixture of two bands (blue and green) to detach the difference in depth from difference in bottom albedo. The algorithm works on the principle that the observance of water differs from band to band, when the depth of water changes. Generally, the spectral band of green is high in absorptivity, in which the reflected irradiance declines quicker than in the low absorptivity of blue band (Pe'eri et al., 2014). Therefore, the ratio between the green and blue band declines linearly with penetration, when they are log-transformed. It is important to note that both bands are affected similarly with the changes in the bottom albedo. But the high absorption band green is affected more when the depth varies.

The mapping of bathymetry in the clear ocean water is successfully mapped up to the depth of 25 to 30 m by adopting the remote sensing technique (Lyzenga et al., 2006; Eugenio et al., 2015; Mishra et al., 2007). To determine the depth of ocean and marine water environment, the blue and green (visible bands) of spectrum wavelength are selected for remotely sensing bathymetry. In the visible bands, light infiltrates the

water column, and an exponential attenuation of radiance as a function of both depth and wavelength delivers the primary principle for estimating the depth (Gao, 2009).

The satellite imagery with high spatial and rich spectral resolution is important for many remote sensing applications. Therefore, in the present study the spatial resolution of MS image is enhanced using pan-sharpening techniques. The qualitative and quantitative approaches were adopted for the selection of best pan-sharpened image. Further, the effectiveness of improving the spatial resolution of multispectral imagery is studied, by extracting the buildings and by estimating the bathymetry of near-shore ocean.

Chapter 2

LITERATURE REVIEW

2.1 General

The chapter presents the literature available in the area of Pan-sharpening, extraction of buildings and estimation of bathymetry using remote sensing imagery.

2.2 Pan-sharpening

This section provides an overview of the work, contributed by various researchers on pan-sharpening.

(Burt and Adelson, 1983) adopted laplacian pyramid to improve the spatial resolution of multispectral image, which is a multi-scale representation obtained through a recursive low-pass filtering and decimation. The laplacian pyramid decomposition was divided into two steps: the first was gaussian pyramid decomposition; the second was to translate the gaussian pyramid to laplacian pyramid. Each level of the Laplacian pyramid were recursively constructed from its lower level using four basic procedures: Blurring (low-pass filtering), subsampling (reduce size), interpolation (expand in size) and differencing (to subtract two images pixel-by-pixel). This method preserves spectral and spatial distortions in the fused image. However, the method losses some information in the fused image due to the subsampling and interpolation procedure.

(Gillespie et al., 1987) developed brovey transfrom pan-sharpening method, and it was also known as colour normalization transform, the method was based on the chromaticity transform and the concept of intensity modulation. The method BT requires only arithmetical operations without any statistical analysis of filter design. It was de-

veloped to provide contrast in features such as shadows, water and high reflectance areas. However, color distortion problem are often produced in the fused images.

(Chavez and Kwarteng, 1989) developed principal component analysis method to improve the spatial resolution of MS image. PCA is a general statistical technique that transforms multivariate data with correlated variables into uncorrelated variables. The PCA method has the advantage that it does not have the three band limitation and can be applied to any number of bands at a time. However, the method introduces spectral distortion in the fused image.

(Carper et al., 1994) employed IHS method to improve the resolution of MS image. The intensity represents the total amount of the light in a colour, the hue is the property of a colour determined by its wavelength, and the saturation is the purity of the colour. The method cannot decompose an image into different frequencies in frequency space such as higher or lower frequency. Hence the IHS method cannot be used to enhance certain image characteristics. However, the method severely distorts the spectral values of the original colour of the MS image. Thus IHS technique is good only for visual analysis, and not for machine classification based on the spectral signatures of the original MS image. Moreover, the method limited to three bands at a time.

(Kingsbury, 1999) adopted undecimadted algorithm to solve the shift-variance problem which was caused by the decimation process. It does by suppressing the down-sampling step of the decimated algorithm using zeros between the filter coefficients. As with the decimated algorithm, the filters were applied first to the rows and then to the columns. In this process, four images were produced (one approximation and three detail images) at half the resolution of the original image. The approximation images from undecimated algorithm represents the spatial resolution becoming coarser at each higher level and the size remains as the original image. It also requires more space to store the results of each level of transformation and although it is shift-invariant it does not resolve the problem of feature orientation.

(Laben and Brower, 2000) developed gram-schmidt transformation method. In this process, the spatial resolution of panchromatic image was simulated and employed as the first band in the gram-schmidt transformation. The statistics of the higher spatial res-

olution panchromatic image were adjusted to match the statistics of the first transform band resulting from the gram-schmidt transformation and the higher spatial resolution panchromatic image (With adjusted statistics) is substituted as the first transform band to produce a new set of transform bands. Finally, the inverse gram-schmidt transformation is performed on the new set of transform bands to produce the enhanced spatial resolution multispectral image.

(Petrovic and Xydeas, 2004) developed gradient pyramid method to obtain high spatial resolution of multispectral image using a set of 4 directional gradient filters (horizontal, vertical and 2 diagonal) to the gaussian pyramid. At each level, these 4 directional gradient pyramids were combined together to obtain a combined gradient pyramid which was similar to the laplacian pyramid. The gradient pyramid fusion is same as laplacian pyramid except replacing the laplacian pyramid with the combined gradient pyramid. The method demonstrated fused image with minimum loss of colour distortion, however it generates the loss of edge information in the fused image.

(Gonzalez-Audicana et al., 2005) adopted non-separated algorithm for dealing with shift variance problem using two-dimensional wavelet filter derived from the scaling function. This produces only two images, one approximation image, and one detail image, called the wavelet plane. The wavelet plane was computed as the difference between the original and the approximation images which contains all the loss of information , from the result of the wavelet decomposition. A coarser approximation is achieved using up-sampling the filter at each level of decomposition; correspondingly, the filter was down-sampled at each level of reconstruction. Some redundancy between adjacent levels of decomposition was possible in this approach, but since it was not decimated, and not involve separate filtering in the horizontal and vertical directions, it better preserves feature orientation.

The major problem with the above standard discrete wavelet transforms was the poor directional selectivity, meaning poor representation of features with orientations that are not horizontal or vertical, which is a result of separate filtering in these directions.

(Fowler and Member, 2005) developed dual-tree complex wavelet transform to overcome the above major problem of discrete wavelet transform. The DT-CWT was a complete wavelet transform which provides both good shift invariance and directional selectivity over the DWT, two fully decimated trees are produced, one for the odd samples and one for the even samples generated at the first level. The DT-CWT has reduced over completeness compared with the signal invariance discerete wavelet transform, and increased directional sensitivity over the DWT and was able to distinguish between positive and negative orientations. Therefore DT-CWT better preserves feature in the fused image. This method is limited to an increased memory and computational cost.

(Amolins et al., 2007) adopted conventional discrete wavelet transform using decimated algorithm. In the decimated algorithm the signal was downsampled after each level of transformation. Down-sampling was performed by keeping one out of every two rows and columns, and generated the image with one quarter of the original size and half the original resolution. In this method, filtering and down-sampling were first applied to the rows of the image and then to the columns. This produces four images at the lower resolution, one approximation image and three wavelet coefficient or detail images. Drawback of decimated algorithm is not shift-invariant, which means that it was sensitive to shifts of the input image. The decimation process also has a negative impact on the linear continuity of spatial features that do not have a horizontal or vertical orientation. These two factors tend to introduce artefacts in the fused image.

(Gangkofner et al., 2008) proposed high pass filter additive fusion method which inserts structural and textural details of the higher resolution image into the lower resolution image, whose spectral properties are thereby retained largely. In this process, various input image pairs, workable sets of HPFA parameters have been derived with regard to high-pass filter properties and injection weights. Improvements are the standardization of the HPFA parameters over a wide range of image resolution ratios and controlled the trade-off between resulting image sharpness and spectral properties. The results of HPFA were evaluated visually and also using spectral and spatial metrics. In comparison with wavelet-based image fusion, it was concluded that proposed method HPFA outperformed.

(Yang et al., 2010) developed a counterlet transform image analysis tool, which was anisotropic and has good directional selectivity. This method can accurately represent the edge information of image with different scales and different direction frequency sub-bands. Contourlet transform is a multi-scale and multi-direction framework of discrete image. In the transform, the multiscale analysis and the multi-direction analysis were separated in a serial way. The laplacian pyramid was first used to capture the point discontinuities, and then directional filter bank was used to link point discontinuities into linear structures. The pyramidal filter bank structure of the contourlet transform has fewer redundancy. However, designing best filters for the contourlet transform was a difficult task. In addition, due to down samplers and upsamplers present in both the laplacian pyramid and the DFB, the contourlet transform is not shift-invariant, therefore it tends to introduce artefacts in the fused image.

(Padwick et al., 2010) proposed a hyperspherical colour space method which accepts any number of input bands. For an image with N bands, one forms a single intensity component and N-1 angles on the hypersphere. Ten different World View-2 satellite images which representing a variety of land cover types were used. The results of HCS method were quantitatively compared with the methods like PCA and GS methods. It was concluded that HCS method is outperforming the other methods.

(Ashraf et al., 2012) proposed subtractive resolution merge which belongs to a new class of data fusion techniques that uses a mix of both spatial and spectral centric approaches. SRM produces a low-resolution panchromatic synthetic image from the weighted sum of the low resolution multispectral image. The LRPISYN was then up-sampled to a HRPISYN and then subtracted from HRPI (which is not synthetic) provides the edge details. The SRM also uses a mix of high pass filter and low pass filter to control spatial details. The results of SRM method were quantitatively and qualitatively compared with conventional techniques like BT, principal component substitution, local mean and variance matching, optimised high pass filter and concluded that SRM method was performed better than other techniques.

(Chai et al., 2012) proposed an nonsubsampled contourlet transform to overcome the limitation of contourlet transform. NSCT transform divided into two shift-invariant

parts: 1) a nonsubsampled pyramid structure that ensures the multiscale property and 2) a nonsubsampled DFB structure that provides directionality. The combinations of these two can preserve more detail in source images and further improve the quality of fused image. The multiscale property of the NSCT was obtained from a shift-invariant filtering structure that achieves sub-band decomposition similar to that of the laplacian pyramid. The NSCT was a fully shift-invariant, multiscale and multidirection expansion which has a fast implementation. The design problem was much less constrained than that of contourlets. This enables NSCT to design filters with better frequency selectivity there by achieving better sub band decomposition. NSCT provide a framework for filter design that ensures good frequency localization in addition to have a fast implementation through ladders steps. However, the method do not represent the source images effectively and completely.

(Yusuf et al., 2012) compared the effectiveness of five fusion techniques such as GS, HPF, M-IHS, Fast Fourier transforms - enhanced IHS and W-PCA. The result of this techniques were evaluated through visual inspection, histogram analysis and correlation analysis. It was concluded that the GS method followed by HPF yields the best quality information in the fused image. The study further suggested that GS and HPF method was suitable for improving visual interpretation and data quality from the viewpoint of remote sensing applications.

(Ghosh and Joshi, 2013) compared and assessed 12 fusion techniques, namely BT, Ehlers, GS, HCS, HPF, M-IHS, multiplicative, PanSHARP, PanSHARP2, PC, W-PCA and W-IHS. The result of these methods were evaluated using qualitative and quantitative analysis. It was concluded that the HPF and PanSHARP methods produced the most visually appealing images, whereas quantitative values indicated that HCS, HPF, and PanSHARP methods performed better than other methods.

(Du et al., 2013) investigated the impacts of different pan-sharpening techniques like GS, PCA, GIHS, WT, and HPF on change detection analysis. The result of different fusion techniques on change detection were evaluated using unsupervised similarity metric and supervised accuracy indices. Comparing the average similarities of change maps from different pan-sharpening techniques, it was found that the GS gets the high-

est score and others were ranked from high to low as: PCA, GIHS, WT, and HPF. Therefore, the overall accuracy of change detection was increased using image fusion techniques.

(Jiang and Wang, 2014) proposed a morphological component analysis which believes that an image contains structures with different spatial morphologies and can be accordingly modeled as a superposition of the cartoon and texture components, and that the sparse representations of these components can be obtained by some specific decomposition algorithms, which exploit the structured dictionary. MCA employs the morphological diversity of an image and provides more complete representation of an image. He compared MCA fusion results with six single-component fusion methods, the results of this method are evaluated through visual inspection and quantitative methods; thus show that proposed method can produce better fused images when compared with other single-component fusion methods.

(Leung et al., 2014) proposed an improved adaptive intensity-hue-saturation in which the amount of spatial detail was injected into each band of the multispectral (MS) image which was appropriately determined using weighting matrix on the basis of the edges of the panchromatic and the proportions between the MS bands. The results of AIHS method were evaluated using both visual inspection and quantitative analysis. It was concluded that the AIHS method can maintain good spectral quality and best spatial quality in the fused image.

(Cheng et al., 2015) proposed a pan-sharpening method, which combines the wavelet transform and sparse representation. Firstly, IHS transform was applied to the MS image. Then, the wavelet transform were used to the intensity component of MS image, the Pan image to construct the multi-scale representation respectively. Sparse representation with training dictionary was introduced into the low-frequency sub-image fusion. Finally, the fused results were obtained through inverse wavelet transform and inverse IHS transform. The wavelet transform has the ability to extract the spectral information and the global spatial details, while sparse representation can extract the local structures of images effectively. The experimental results demonstrated that proposed method was maintained the spectral characteristics of fused images with a high spatial resolution.

(Nejati et al., 2015) proposed a novel multi-focus image fusion method in spatial domain that utilizes a dictionary which were learned from local patches of source images. Sparse representation of relative sharpness measure over this trained dictionary were pooled together to obtain the corresponding pooled features. Correlation of the pooled features with sparse representations of input images produces a pixel level score for a decision map of fusion. Finally, a regularized decision map was obtained using MRF optimization. The result of proposed method outperforms existing state-of-the-art methods, in terms of visual and quantitative evaluations.

(Xu et al., 2015) proposed a regression based fusion method. This method was proposed to overcome the problem of component substitution, which assumes a linear relation between Pan and MS images. Due to the nonlinear spectral response of satellite sensors, the qualified low-resolution Pan image cannot be well approximated using weighted summation of MS bands, which leads to significant gray value difference between a Pan and MS images. The proposed method divides Pan and MS images into several pixel groups using k-means algorithm. Then, the low-resolution Pan image was estimated using weighted summation of MS bands on each groups of classified pixel. Finally, the fused image was generated by ratio enhancement method. Experimental results demonstrated that the proposed technique can provide significant improvements in reducing color distortion.

(Song et al., 2015) proposed learning-based super-resolution method to fuse two data types such as Landsat TM and SPOT 5. They first modeled the imaging process from a SPOT image to a TM/ETM+ image at their corresponding bands, by building an image degradation model via blurring and down sampling operations. In the proposed method two important steps to fuse the images are, 1) learning a dictionary pair representing the high and low resolution details from the given SPOT5 and the simulated TM/ETM+ images; 2) super resolving the input Landsat images based on the dictionary pair and a sparse coding algorithm. To examine the performance of the proposed method, the classification experiment was implemented on the input image and fused image. It was concluded that the accuracy of fused image classification outperforms the input image classification.

The major driving force for research in the domain of Pan-sharpening, is to overcome the technical problem of satellite sensors (Pan and MS) which are not able to acquire a single image with a high spatial and rich spectral information. Further, most of the remote sensing applications such as change detection analysis, LULC and detection of buildings requires both high spatial and rich spectral information in a single image. Therefore, to achieve the both qualities in a single image many pan-sharpening methods were developed and utilized for fusing the Pan and MS imagery.

Generally, pan-sharpening methods like PCA, M-IHS, BT, Multiplicative, W-PCA, HCS, HPF and GS were widely used for fusing the Pan and MS imagery for various remote sensing applications. The M-IHS method works by substituting the intensity component with the Pan image and attains the pan-sharpened image by an inverse M-IHS transformation, the results of this method generally preserves spatial detail of the Pan image, at the same time it generates some spatial and spectral distortion. While, other pan-sharpening methods like PCA, HCS and GS also generates the spatial and spectral distortion. For instance, the PCA method generates the spatial and spectral distortions. The PCA method often generates the pan-sharpened image with exaggerated information. The method BT provides the excellent spatial detail but generates the high spectral distortion. By comparison, the GS method generates the more spatial detail by improving the concentration of Pan band, however the spectral distortions occurs frequently in the pan-sharpened image, the HCS method can generates the pan-sharpened image with high spectral fidelity, but it generates blurred spatial information.

The main constrains of these pan-sharpening methods are severe spectral distortion (i.e. spectral information presents in the original MS) is not retained completely during fusion process. For example, the red vegetation in the original MS image changed to black color after fusion. To overcome spectral distortion, several methods like HPF and wavelet have also been attempted, the HPF methods produces a fused image with less spectral distortion, but often generates the spatial distortion for the reason of combination between the spectral and spatial information is not smooth. The wavelet based methods better preserves the spectral information because of their ability to describe and retrieve the spatial and spectral information in different scale. However, detailed

coefficients components are injected to each MS bands, the method sometime produces the artefacts in fused image through a high pass filter. The satellite image with high spatial and rich spectral information is required for remote sensing applications. Moreover, the availability of satellite images acquired by advanced sensors has improved the spatial resolution of the Pan and spectral resolution of MS images. Therefore, it is necessary to adopt the new pan-sharpening algorithm and compare with the widely used pan-sharpening algorithms using qualitative and various quantitative approach.

The results of pan-sharpening methods requires quality analysis, before they adopted for remote sensing applications. Generally, qualitative and quantitative analyses were used for the evaluation of spatial and spectral quality of fused image. One of the major limitation observed in the pan-sharpening studies was that the performance of many existing pan-sharpening algorithms were compared and assessed using limited quantitative analysis. Therefore, it is necessary to evaluate the quality of pan-sharpened using qualitative and various quantitative approach and the selection of best pan-sharpening method can be applied for remote sensing applications like extraction of buildings and estimating the bathymetry of near-shore ocean.

2.3 Extraction of buildings

This section provides an overview of the work, carried out by various researchers on the extraction of buildings.

(Attarzadeh and Momeni, 2012) proposed a new automatic algorithm based on object approach for the detection of buildings from the satellite imagery. Here, the stable and variable features were utilised jointly; the stable features were obtained from the inherent qualities of building phenomenon and the variable features were detected using separability and threshold analysis tool. The proposed algorithm was adopted on Quickbird imagery and the visual analysis indicate that the proposed algorithm can detect major rectangular buildings clearly.

(Wang et al., 2013) proposed a novel approach using corner detection, segmentation and adaptive windowed Hough transform for detecting buildings from Quickbird satellite imagery. Firstly, the input image was segmented into a number of classes us-

ing a mean shift segmentation algorithm. Secondly, the corners of the buildings were extracted using the scale invariant feature transform. Finally, extraction of building was achieved using adaptive windowed hough transform. The visual analysis indicates that the proposed method can detect buildings with rectangular shape.

(Ghaffarian and Ghaffarian, 2014) Detected buildings from high resolution Google earth image using the following process: At first, the shadow areas were detected and masked using novel double threshold method. Training samples for performing the supervised classification were chosen automatically by forming a buffer zone for each building. The statics value for each buffer zone was calculated to perform the improved parallelepiped supervised classification for the detection of buildings further, the parallelepiped classification method and morphological operators were adopted to improve the overall accuracy. The pixel and object based performance of proposed method was evaluated quantitatively. The proposed method can detect the buildings without influencing from their geometric characteristics and also it provides the training data sample automatically to the supervised classification. However, the method classifies the non-buildings features as building features, when they have equivalent spectral values.

(Liasis and Stavrou, 2016) developed a framework based on the active contour segmentation, processed by analysing the properties of RGB representation and the holdings of HSV were used to extract the buildings from the satellite image. Initially, the vegetation and shadow features were removed using the clustering technique. The new active contour model was developed, based on the HSV representation of the image to attain superior segmentation, a new energy span was encoded for biasing the contour. Finally, the morphological operator was adopted to remove misleading information. Both, qualitative and quantitative analyses were performed to estimate the performance of proposed method. The proposed method detects the buildings with arbitrary shapes and sizes. A limitation of the proposed method was that some non-building objects like bridges, roads were classified as buildings. Further, buildings which are close to each other were classified as a single building. Moreover, the performance of proposed method is depend on the assessment of structural element size for the morphological operation like erosion and dilation.

(Chaudhuri et al., 2016) introduced a novel framework for extracting the buildings from high-resolution Pan imagery of Quickbird-2 and Ikonos. The key steps in the framework are: Firstly, the input image was enhanced using morphological operator to improve the visual effect and also to differentiate the targeted object from the non targeted object. Secondly, multiseed based clustering technique using internal gray variance were used to separate the man-made features from the non man made features. The presence of shadow from the flat road feature was detected and separated from the buildings using positional information of both building edge and shadow. Later, adaptive threshold based segmentation technique was used to segment and to extract the buildings from the input image. A limitation of proposed method was that, if the top of the building is partially bright and partially dark, then this technique will detect only a part of the building. This occurs for the reason that proposed segmentation algorithm works based on the threshold value for a specific region of interest. The proposed approach relies on the shadows of the buildings to accurately locate the buildings, images with low rise buildings in urban area do not have sufficient shadows in that situation the buildings are not detected accurately.

In previous studies, buildings were extracted using google earth image, Pan image, and MS image with the combination of R, G, and B color mode. Majority of algorithms work efficiently for detecting buildings with the same shape (i.e. rectangular, square), colour and size. The major driving force for research in the domain of building extraction, is to extract the buildings from the MS image with the combination of R, G, B and NIR color mode, in which buildings are in different shapes, colours and sizes. However, high spatial resolution and rich spectral information is important and required to obtain high spatial and rich spectral information of buildings. Therefore, it is necessary to address these limitations by pan-sharpening techniques and to frame a methodology for the extraction of buildings with different shapes, sizes and colour.

2.4 Bathymetry mapping

The section provides an overview of important literature, contributed by a number of researchers for estimating the bathymetry of ocean using remote sensing technology

and is discussed below:

(Lyzenga et al., 2006) proposed a physically based algorithm to determine the bottom depth of ocean. The algorithm corrects the range of variations in both water attenuation and bottom reflectance using linear combination of log-transformed radiances in the blue and green channels. The proposed algorithm were adopted to different regions like Hawaii, Cancun and Mexico using Ikonos satellite imagery. The performance of the proposed algorithm was compared with ground-truth measurements using RMSE indices and the value of RMSE revealed that the proposed algorithm results well co-related to the ground-truth measurements.

(Su et al., 2008) developed an automated method for calibrating the parameters for a non-linear inversion model based on the Levenberg-Marquardt optimization algorithm for determining the bathymetry of south shore of Molokai Island, Hawaii using Ikonos satellite imagery. Depth data derived from the non-linear inversion model were compared with the conventional log-linear inversion model. It was observed that the overall performance of both the models were similar. The study concluded that the non-linear inversion model produced slightly better and accurate estimation of deeper depth of 10-15 m, but slightly less accurate for very shallow regions (i.e. $<$5 m).

(Sheng et al., 2014) proposed a linear logarithm ratio model for estimating shallow water depth from hyperspectral data. The proposed method was based on the different responses of shallow water reflectance of depth and substrate type. Two parameters like similarity coefficient and pearson correlation coefficient was used to model a linear logarithm ratio algorithm. The results of the proposed algorithm were validated using RMSE indices. The value of RMSE indicate that the proposed method was capable to estimate the depth $>$20 m in shallow water.

(Su et al., 2014) used a geographically adaptive inversion and conventional global inversion model to estimate the bottom depth over Kauai and Barbuda Island using high resolution Ikonos and Landsat ETM+ satellite imagery. The performance of conventional global inversion model was limited, when the bottom type and water quality vary spatially within the scene. The geographically adaptive inversion model divides the image scene into local areas to calibrate the inversion models for each submission

to improve the accuracy and reliability of retrieving the bathymetry from remote sensing imagery. It was demonstrated that the geographically adaptive inversion model estimates the bathymetry better than the conventional model.

(Eugenio et al., 2015) implemented the multichannel physical s-based algorithm to determine the bathymetry of Granadilla (Tenerife island) and Corralejo (Fuerteventura island) areas using Worldview-2 imagery. To retrieve the depth accurately, the physical s-based algorithm was coupled with radiative transfer model. The coupled model estimates the depth effectively up to 25 m. The model declines the prediction of depth greater than 25 m.

(Vahtmäe and Kutser, 2016) investigated linear band model and the log-transformed band ratio model for determining the bathymetry of optically complex Baltic sea region using airborne Hyspex Hyperspectral images. The results of the models were compared using statistical indices like R^2 and RMSE. The value of these indices indicate that the linear band model was outperformed the log-transformed band ratio model by accurately estimating the depth of 4 m. The log transform model provides inaccurate results for the reason of high albedo in the near coastal regions.

The following literature represents the estimation of bathymetry along the coast of India:

(Pattanaik et al., 2015) used a simple radioactive model and linear radioactive model for estimating the depth along the coast of Odisha, India using IRS LISS-III multispectral imagery. The statistical indices R^2 was used to compare the result of two models. The indices value indicated that the linear radioactive model outperformed the simple radioactive model. It was concluded that both the methods were effective to determine the depth of 4-5 m.

The major driving force for research in the domain of bathymetry, is to frame the procedure to estimate the bathymetry of near-shore ocean using Landsat-8 satellite imagery. Generally, bathymetry of near-shore ocean was established using in-situ instruments which are expensive. Therefore, immense focus has been on application of satellite imageries due to their global coverage, which addresses the limitation associated with the in-situ instruments. Satellite data also have limitations, but they are subsided

by the advantages like - global coverage, low or free cost of data. The existing literature (globally) provided detailed information of the estimation of bathymetry using remote sensing data. It is noted that, bathymetry study using remote sensing data was small in number (Indian scenario). Moreover, in an ocean port it is mandatory to maintain certain depth throughout the year for the smooth transportation of large ships. The in-situ instruments used in the ports to maintain the depth is limited by its high purchasing and maintenance costs. Therefore, it is necessary to address these limitations with satellite-based data and a methodology to assess the batyhmetry of near-shore ocean that can be applied to other sites.

The literature survey carried out under each section, helped in gathering vital information on the existing and current research in the domain of pan-sharpening techniques, algorithm for the extraction of building and also for estimating the bathymetry of ocean.

For many remote sensing applications it is necessary to have both high spatial and rich spectral information in a single image. For this purpose many pan-sharpening algorithms have been developed and the selection of best pan-sharpening method is challenging. Therefore, it is necessary to study the effectiveness of widely used pan-sharpening algorithms with the new pan-sharpening algorithm, using qualitative and various quantitative approach. Further effectiveness of improving the spatial resolution of multispectral image is needed to be addressed by extracting the buildings and by estimating the bathymetry of near-shore ocean.

2.5 Problem formulation

As discussed in section 2.2 to 2.4, the two sensors Pan and MS have both advantages and disadvantages: Pan sensor provides the Pan image in a single band, with high spatial resolution but it cannot provide images in multiple bands with high spectral resolution, whereas MS sensor can provide images in multiple bands which contains a rich spectral resolution but low spatial resolution. Further, it was seen that there are two technical constraints of the sensor to deliver an image with both high spatial and rich spectral resolution- i) Quantity of radiation energy received by the sensor, ii) amount of information collected by the sensor. Therefore, earth observation satellites like Landsat

and Quickbird series, provide simultaneously low spatial and high spectral resolution of MS image and high spatial and low spectral resolution Pan image.

Hence to overcome this constraint, the pan-sharpening algorithms is proposed to be adopted in the present work such as PCA, M-IHS, BT, multiplicative, HPF, W-PCA, HCS, GS and Fuze Go to improve the spatial resolution of MS image. To evaluate the quality of pan-sharpened image, researchers evaluated and compared the efficiency of different pan-sharpening methods using limited quality metrics. Therefore, it is proposed to evaluate the spatial and spectral quality of pan-sharpened image using qualitative and various quantitative approaches.

Further, the effectiveness of improving the spatial resolution of MS image is studied in the present work by extracting the buildings and by estimating the bathymetry of near-shore ocean.

2.6 Objectives of the Study

Based on the literature summary, the objective of the present research is:-

- To improve the spatial resolution of multispectral (MS) imagery of Quickbird-2 and Landsat-8 using pan-sharpening methods.

The scope of the present research is as follows:

- To evaluate the spatial and spectral quality of pan-sharpened image using qualitative and quantitative analysis.
- Extraction of building from the best pan-sharpened image and from the original MS image.
- To estimate the bathymetry of near-shore ocean, before and after improving the spatial resolution of landsat-8 imagery.

2.7 Organisation of thesis

The information congregated from the work is presented in five chapters followed by list of references.

Chapter 1 provides the brief introduction of remote sensing, pan-sharpening, extraction of buildings and bathymetry mapping.

Chapter 2 provides a supporting literature review in the domain of pan-sharpening, extraction of buildings and bathymetry mapping are helped in understanding the concepts. The objectives are thus framed to address the limitations and enhance existing knowledge.

Chapter 3 presents the overall methodology and detailed framework of each objective, detail information on the characteristics of data and study location.

Chapter 4 discusses the results obtained for pan-sharpening methods and quality evaluation of pan-sharpened image using qualitative and quantitative analysis, automatic and manual approach for the extraction of buildings and estimation of bathymetry along the coast of Mangaluru.

Finally, conclusions drawn from the study are presented in Chapter 5 along with limitations and future scope of work.

Chapter 3

MATERIALS AND METHODOLOGY

3.1 General

Remote sensing satellite sensors capture the images of the earth surface and deliver them to the ground station as images, and have gained importance for the global coverage capacity. These imageries can be a source for understanding and identifying the different features. They also help to analyse the changes of features spatially and spectrally over a period of time. The high (spatial) resolution and spectral information is available in (Pan) and MS imageries, respectively. It is necessary for remote sensing applications to have both high spatial and rich spectral resolution in a single image. There are limitations associated with satellite sensors to provide both characteristics in a single image. The pan-sharpening techniques have been focused to enhance the spatial resolution of MS image. On the other hand, the effectiveness of improving the spatial resolution of MS image are required to be emphasized by extracting the buildings and by estimating the bathymetry of near-shore ocean.

The chapter present the overview of the study area, data products and also the overall methodology of the research work. Subsequently, detailed methodology for improving the spatial resolution of MS image, extraction of buildings and for estimating the bathymetry of near-shore ocean is also discussed.

3.2 Study area

The coastal region of Dakshina Kannada district of Karnataka state, India stretches from Talapadi in the south to Baindur in the north over a distance of about 140 Km.

The region is enclosed by the Arabian Sea on the west and the Western Ghats on the east. Generally, the coast of Dakshina Kannada adores the tropical hot monsoon climate due to its latitudinal position. The coast is influenced by the southwest monsoon which receives heavy rainfall during the months from June to September, ranging from 3000 mm to 3900 mm. The coast experiences high temperature throughout the year with relatively constant high humidity. During the monsoon period, wave height of 6.5 m is recorded along the coast of Dakshina Kannada and in the non-monsoon period, the height of wave is less than 1 m.

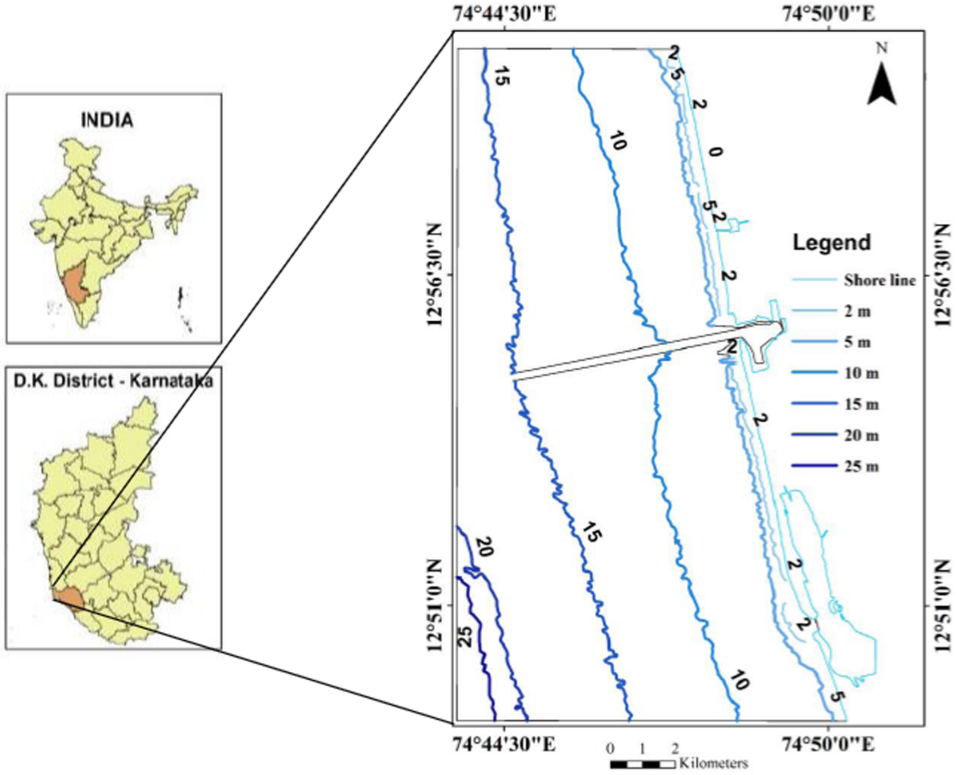

Figure 3.1 Location map of study area

The study area covers the total length of 25 Km extending from ullal region in the south to surathkal in the north roughly $(12°51'0''S74°50'0''E)$ shown in Fig. 3.1. Mangaluru is the major city in the coast of Dakshina Kannada, which gains economic importance due to urbanization and industrialization. The Netravathi and Gurpur rivers originate in the western ghats and flows westward, then it takes a right angle bend

near the coast and then flow north (Gurpur) and south (Netravathi) parallel to the coast. These rivers join together at some point before they merge into the Arabian sea. The study area along the coast of Mangaluru covers the range of depth up to 25 m and also encompasses the New Mangaluru Port Trust.

3.3 Data used

In the present study, two different sets of satellite imageries acquired from Quickbird-2 and Landsat-8 were fused separately. In this process, certain important conditions must be satisfied (Fonseca et al., 2008): a) Both Pan and MS images must have been captured at the same time and should encompass the same expanse; b) the spectral range of the Pan and MS images should be in the same range of wavelength or as close as possible.

A high-resolution imaging satellite named Quickbird-2 was launched on October 18, 2001. Quickbird-2 acquires five bands covering Pan, B, G, R and NIR. The specifications of Quickbird-2 imagery are shown in Table 3.1. The satellite sensor captures the Pan image with a high spatial resolution of 0.60 m and MS image with high spectral resolution but a low spatial resolution of 2.4 m as shown in the Figs. 3.2(a) and (b). The re-sampled MS image to the size of the Pan image is shown in Fig. 3.2(c).

The data location is the opera house in Sydney, Australia $(33°51'25''S151°12'55''E)$ provided by DigitalGlobe. The wavelength range of four bands such as B, G, R and NIR matches with the Pan band thus, all four bands are layer stacked to obtain the MS image. The image of Quickbird-2 covers the features like commercial buildings, urban area, road, vehicles, water, roof, tree, grass and shadows. In the MS image the shape of the vehicles, building roofs are not easily identified; on the other hand, these are easily recognized in the Pan image. Therefore, enhancing the spatial resolution of MS image of Quickbird-2, helps in increasing the spatial and spectral information of features.

The Landsat-8 satellite, launched on February 11, 2013, acquires 11 bands including Pan, B, G, R and NIR. The specifications of Landsat-8 imagery are shown in Table 3.2. The satellite sensors offer Pan images with high spatial resolution of 15 m is shown in the Fig. 3.3(a) and MS image with rich spectral information, but low spatial resolution

Table 3.1 Specifications of Quickbird-2 imagery

Satellite/sensor name	Bands	Resolution (in meters)	Spectral range (in nanometers)
Quikbird-2/Early Bird Panchromatic (EBP)	Pan	0.61	405-1053
Quikbird-2/Early Multispectral (EBM)	B	2.4	430-545
	G	2.4	466-620
	R	2.4	590-710
	NIR	2.4	715-918

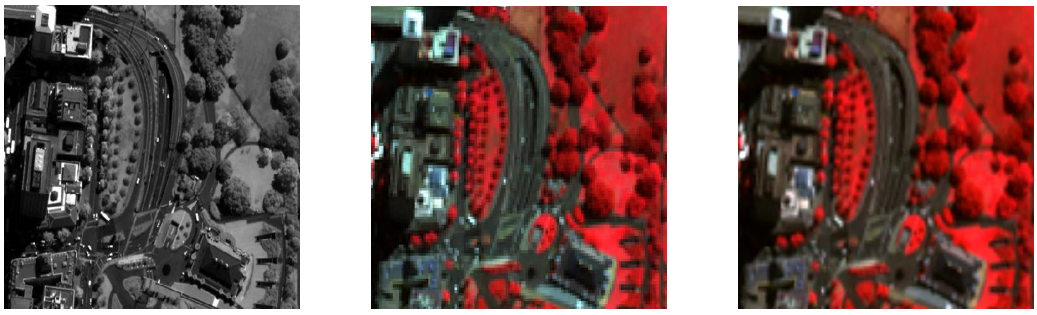

(a) Pan (b) MS (c) Re-sampled MS

Figure 3.2 Quickbird-2 satellite imagery

of 30 m is shown in the Fig. 3.3(b). The re-sampled MS image to the size of the Pan image is shown in Fig. 3.3(c).

The spectral range of bands B, G, and R are close to those of Pan image; therefore, bands B, G, and R were layer-stacked to produce the MS image. The data location is the Mangaluru, Dakshina Kannada district, in Karnataka, India approximately $(12°51'0''S74°50'0''E)$. Landsat-8 imagery is downloaded from the United States Geological Survey (USGS) website (http://www.usgs.gov) acquired during March 13, 2014. The high spectral resolution is observed in the MS image helps to better distinguish the objects like roads and buildings. The high spatial resolution of Pan image leads to accurate delineation of the objects. Therefore the Pan and MS images are fused to obtain

a single image with both high spatial and spectral informations.

The dataset used for the present study satisfies the conditions; therefore, the Pan and MS images of both Landsat-8 and Quickbird-2 were fused using different pan-sharpening techniques.

Table 3.2 Specifications of Landsat-8 imagery

Satellite/sensor name	Bands	Resolution (in meters)	Spectral range (in micrometers)
Landsat-8/Operational Land Imager (OLI)	Pan	15	0.50-0.68
	B	30	0.45-0.51
	G	30	0.53-0.59
	R	30	0.64-0.67
	NIR	30	0.85-0.88

(a) Pan (b) MS (c) Re-sampled MS

Figure 3.3 Landsat-8 satellite imagery

3.4 Methodology

The section delivers overall methodology for executing the present work is shown in the Fig. 3.4. The detailed framework for improving the spatial resolution of MS image is shown in the Fig. 3.5. The methodology of automatic and manual methods for

the extraction of buildings are shown in Figs. 3.10 and 3.11. The methodology for estimating the bathymetry of near-shore ocean is shown in the Fig. 3.12. Subsequently, detailed explanation of each methodology are described.

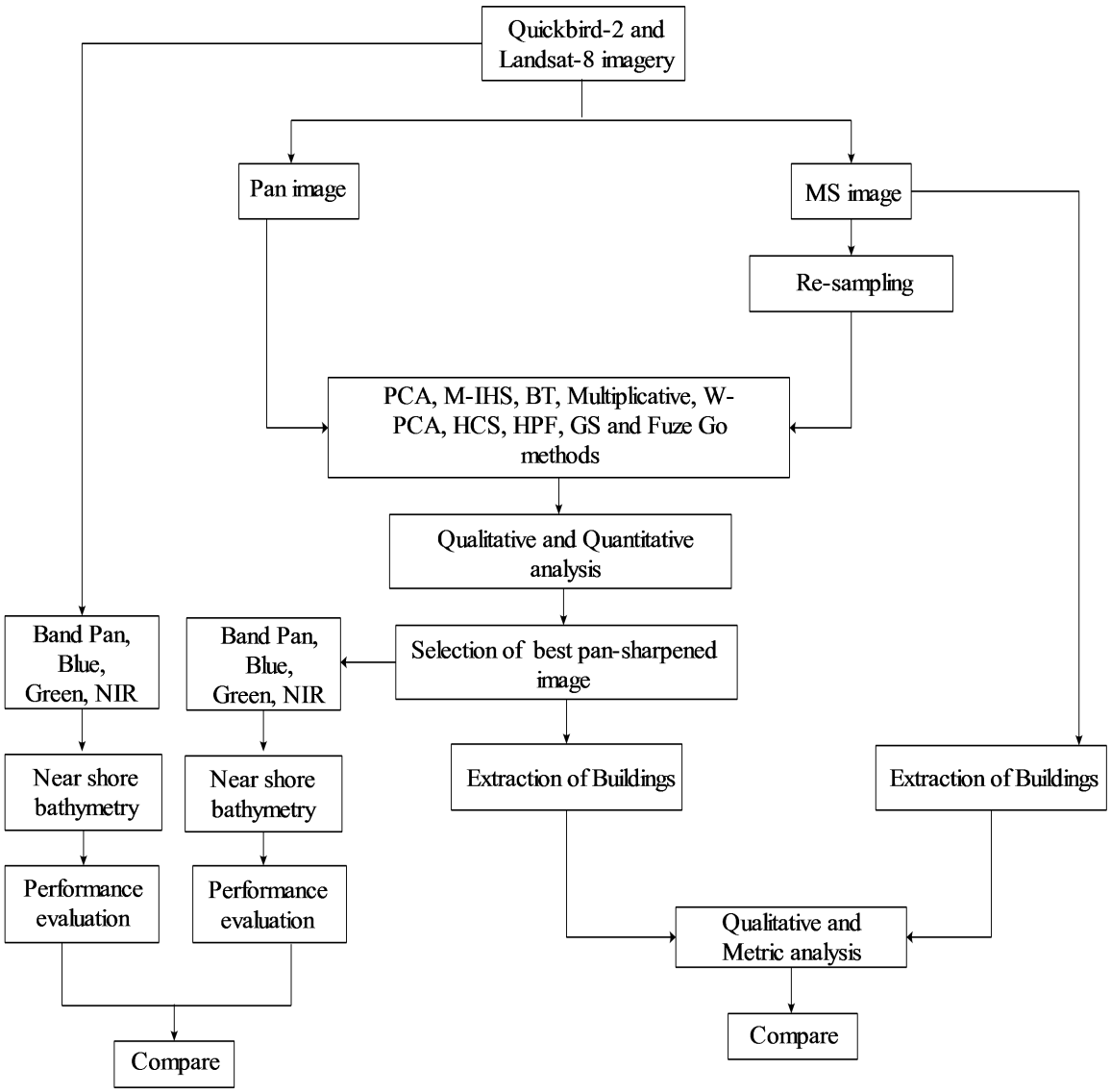

Figure 3.4 Overall methodology of the proposed work

3.5 Pan-sharpening

Pan-sharpening is the process of fusing the high spatial detail of a Pan image and the rich spectral resolution of an MS image. It transfers the spatial information of the Pan

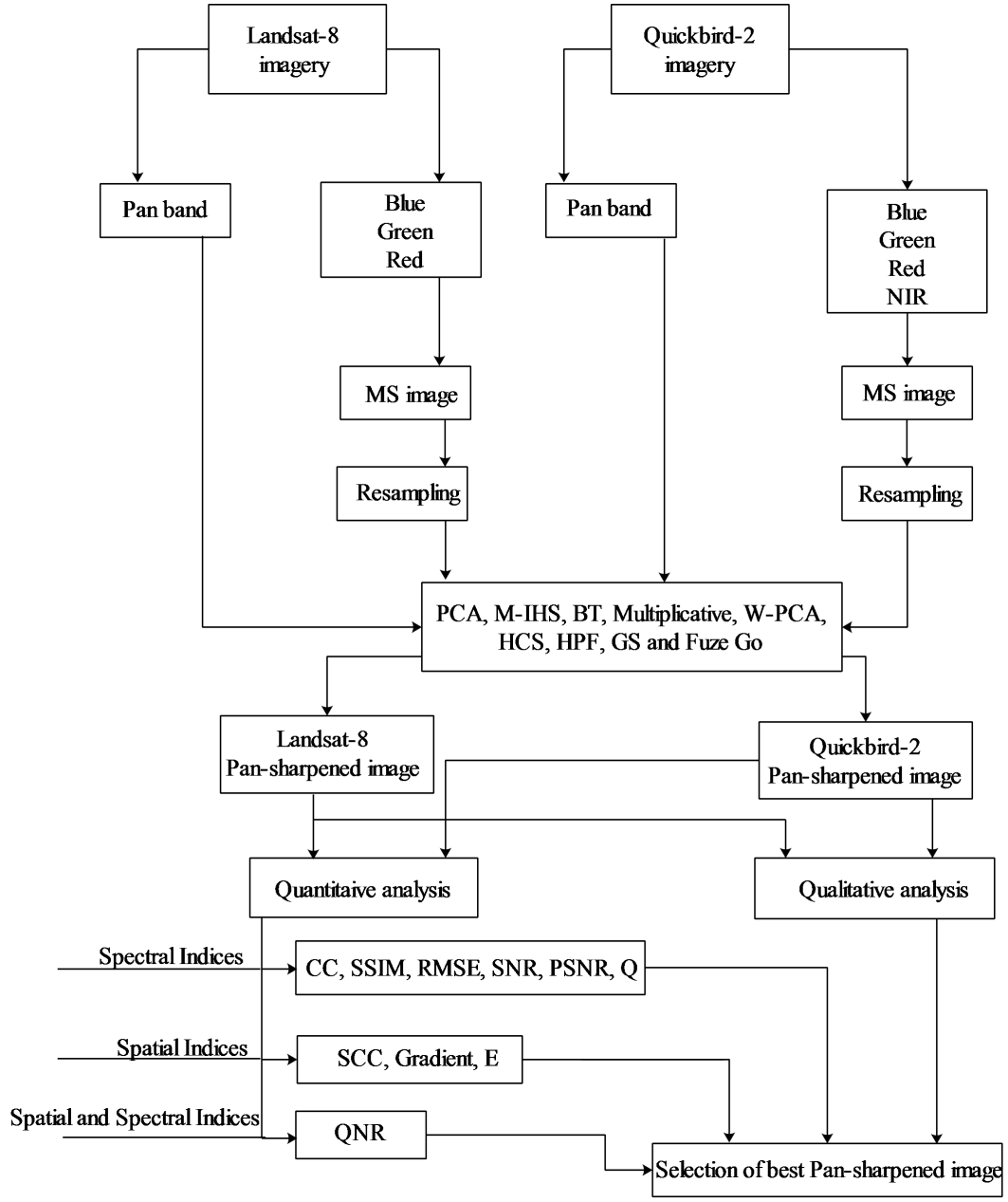

Figure 3.5 Methodology for improving the spatial resolution of MS image

image to the MS image while retaining the spectral data of the MS image for creating a single image with both high spatial and rich spectral information (Zhang, 2010). To improve the spatial resolution of MS image various pan-sharpening algorithms are developed like PCA, M-IHS, BT, Multiplicative, W-PCA, HCS, HPF and GS. These pan-sharpening algorithms were used widely and compared fusing the different set of satellite imageries.

However, advanced remote sensing satellites has improved the acquisition of image with high spatial Pan image and rich spectral MS image. Therefore it is necessary to re-evaluate the above mentioned pan-sharpening algorithms. The existing literature provides the detailed information of fusing the Pan and MS imagery using above mentioned pan-sharpening algorithms. The pan-sharpening study using Fuze Go method were less in number, therefore the effectiveness of Fuze Go method is compared with the above mentioned methods by fusing Quickbird-2 and Landsat-8 imageries. The detailed execution for improving the spatial resolution of MS image are described as below.

3.5.1 Pre-processing

An important requirement for processing the pan-sharpening algorithm is accurate co-registration of Pan and MS image. The dataset of both Pan and MS imageries of Quickbird-2 and Landsat-8 were attained at the same time by the same sensor, therefore the images were fused directly without co-registration (Padwick et al., 2010).

3.5.2 Band selection

The wavelength range of MS bands matches with the Pan band; thus, all the corresponding spectral range of multispectral bands was merged to generate the MS image. Later, the MS image is fused with the Pan image.

3.5.3 Resampling

Up-sampling the original MS image to the spatial resolution of Pan image is important prerequisite for performing many pan-sharpening techniques like PCA, M-IHS, BT, W-PCA, HCS and HPF. The most common resampling methods are nearest neighbour, bilinear interpolation, and cubic convolution. The best suitable resampling methods for pan-sharpening technique was selected on the basis of present literature, as well as recommendation in the software manuals.

3.6 Overview of pan-sharpening techniques

The section discuss the detailed execution of pan-sharpening techniques like PCA, M-IHS, BT, Multiplicative, W-PCA, HCS, HPF, GS and Fuze Go are as described below.

3.6.1 Principal component analysis

Based on a statistical technique, PCA tends to transfer the correlated data into uncorrelated data. In general, PCA transformation is applied on MS images to generate uncorrelated images such as PC1, PC2,..., PCn. Traditionally, this method assumes that the PC1 image is a good indicator of a Pan image; conversely, PC2,..., PCn collect the spectral data of MS images. The uncorrelated PC1 image is replaced by a Pan image with high spatial resolution. Finally, the inverse transformation is applied to obtain a fused image.

3.6.2 Modified-intensity hue saturation

The M-IHS method works by replacing the intensity component with the Pan band. To derive the intensity component, the original spectral bands of the MS image is transferred to IHS. In the first mode, this method replaces the intensity component of the MS image by the corresponding intensity of the Pan band. In the second mode, it reproduces the original MS colours. Thus, this method works best when the wavelength ranges of both Pan and MS images are overlapped. The M-IHS method can be used to merge images of more than three bands by running several passes of the algorithm to fuse the resulting layers.

3.6.3 Multiplicative

The multiplicative method works by processing a simple multiplicative algorithm. The following equation is used to merge the Pan and MS images.

$$(DN_{Pan}) \times (DN_{MS}) = DN_{newMS} \tag{3.1}$$

The equation is simple and one of the quickest methods for fusing two different datasets. It requires the least amount of resources for running the algorithm effectively. In general, this method increases the intensity component in merged image, which have

a tendency to highlight the urban features; hence, it is desirable for urban studies. However, the multiplicative method cannot contain the radiometric information of the MS image in the fused image.

3.6.4 Brovey transform

The BT method generates a new MS image with the spatial detail of Pan image by multiplying the individual pixels of each low spatial resolution band of the MS image by the ratio of the high spatial resolution of the Pan image and dividing by the sum of the MS images. This method generates visually appealing images by improving the contrast of the lowest and highest ends of the histogram of an image. However, it fails to prevent the radiometric data of the original MS image from appearing in the fused image, and it can fuse only three bands at a time. The general mathematical formula of BT based fusion is

$$DN(i)_{fused} = \left[DN(i) \Big/ \sum DN(i) \right] \times DN_{Pan} \tag{3.2}$$

3.6.5 Wavelet-principal component analysis

The W-PCA method is a hybrid of wavelet and PCA. The procedure of this method can be stated as follows: PCA is applied to the MS image to obtain the first principal component (PC1). Histogram match the Pan image to the PC1 image. Decimated wavelet decomposition is applied to the histogram matched Pan and PC1 images. During this process, Daubechies 4 wavelet coefficients are applied to the Pan and PC1 images to obtain an approximation image with three wavelet coefficient sub-images corresponding to horizontal decomposition , vertical decomposition , and diagonal decomposition. By using the inverse multi-resolution wavelet decomposition, the coefficients of the Pan image are inserted into the PC1 image, and inverse PCA transform is applied to the PC1 image to obtain an MS image with the spatial detail of the Pan image. A common flow chart for W-PCA method is shown in Fig. 3.6.

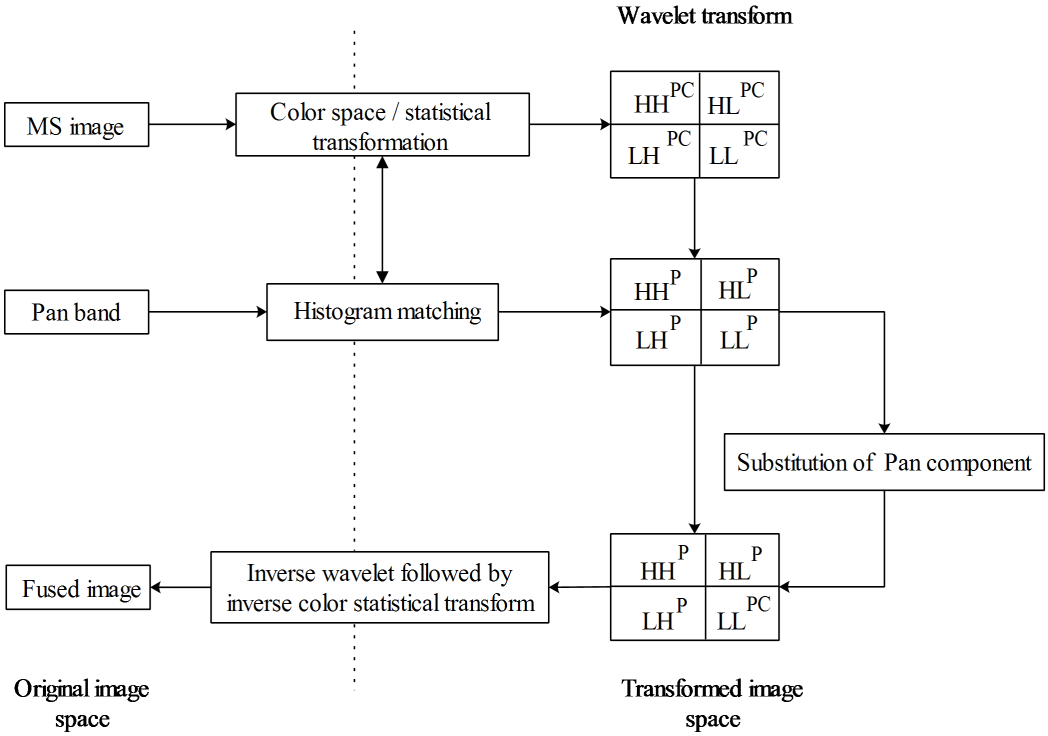

Figure 3.6 General flow chart for W-PCA method

3.6.6 Hyperspherical colour sharpening

The HCS method works by transforming the MS image to a new color space, in which the intensity is orthogonal to the color information. During the transformation, the intensity of multispectral image is matched to the intensity component of Pan image. The histogram-matching is employed to minimize the intensity difference between Pan and MS image. Further, the intensity component of the MS image is replaced by the corresponding intensity form of the Pan band. The reverse transformation is employed using the substituted intensity component transform back to the original color space. The HCS fusion process has the advantage of merging more than three bands.

3.6.7 High pass filter

The HPF technique is an enhanced version of wavelet resolution merge, which requires less computational time and data space. The overall processing of the HPF algorithm is described as: The ratio R is computed between the pixel size of the Pan and MS images. A small high pass filter is placed on the Pan image, and the pixel size of the MS image

is resampled to that of the high pass Pan image. The filtered high pass Pan image is added to the resampled MS image to obtain a merged image with both high spatial and rich spectral information. The common flow chart of HPF method is shown in the Fig. 3.7.

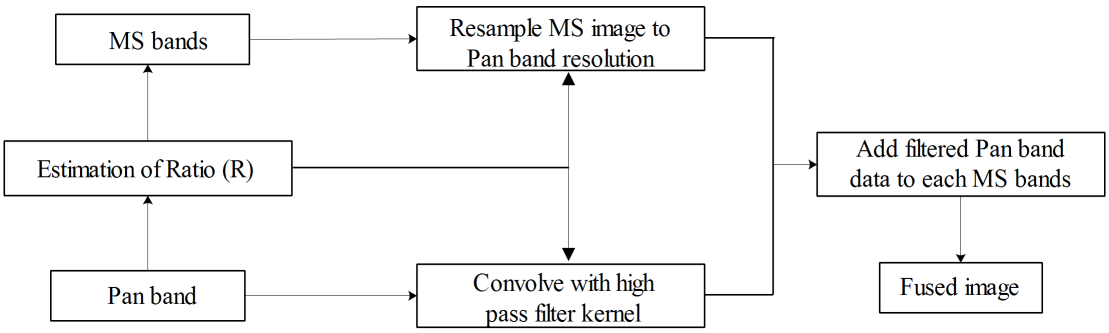

Figure 3.7 General flow chart for HPF method

3.6.8 Gram-schmidt

The GS method was developed to sharpen the spatial resolution of MS images while preserving the spectral qualities of the MS image. The process of this method can be described as: The Pan band is simulated to the lower spatial resolution of the MS band through the weighted sum of the MS bands. The weights of the MS bands are determined from the sensors optical diffusion and from the spectral ranges of the MS and Pan bands. GS transformation is executed on the simulated Pan and MS bands by using the simulated Pan band as the first band. The statistics of the high pixel-sized Pan band are adjusted to balance the statistics of the first band of the GS transformation. Then, the first band of the GS transformation is replaced with the adjusted high spatial detail of the Pan band. Finally, inverse GS transformation is applied to generate a MS image with the spatial resolution of the Pan image. The common flow chart of GS method is shown in the Fig. 3.8.

3.6.9 Fuze Go

A common flow chart for the Fuze Go method is shown in Fig. 3.9. The Fuze Go method achieves a pan-sharpened MS image by implementing the following process:

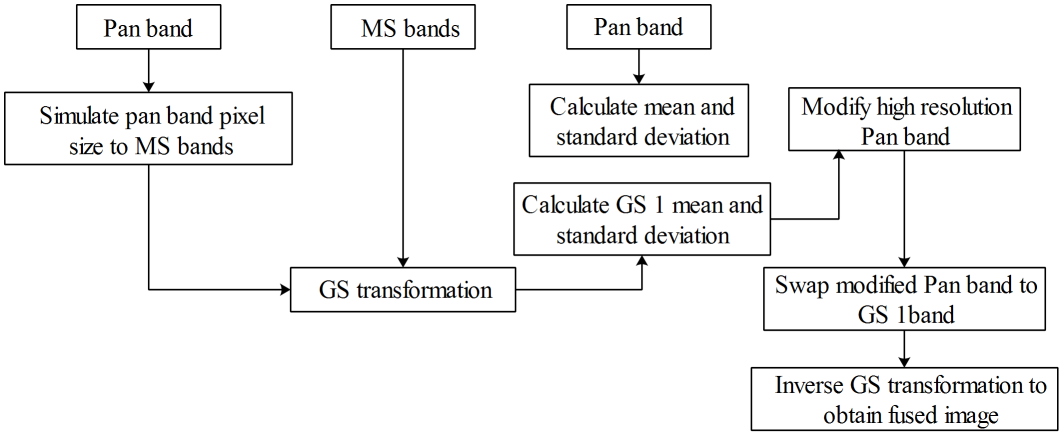

Figure 3.8 General flow chart for GS method

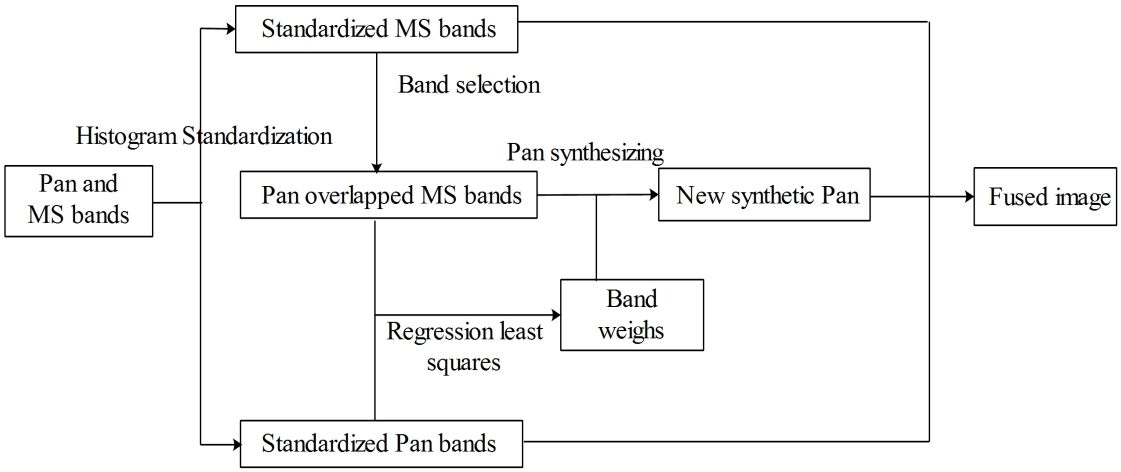

Figure 3.9 General flow chart for Fuze Go method

The MS bands having a spectral range equal to that of the Pan band are selected. Standard deviation, mean, and covariance are calculated for both the selected MS bands and the Pan band. Then, histogram standardization is implemented on both bands. By implementing the mean and standard deviation, all of the selected sets of MS and Pan bands are standardized. The coefficient values are computed by applying the selected MS and Pan bands. Band weights calculated from the covariance matrix are applied for simulating a synthetic Pan band. Subsequently, a synthetic Pan band is created by applying the selected MS bands and set weights. The product-synthetic ratio is determined by applying the standardized Pan band, standardized MS bands, and synthetic Pan image to obtain the fused image.

3.7 Quality assessment of fused image

Pan-sharpening is the process of transferring the spatial information of a Pan image to an MS image to generate an image with enhanced spatial detail equal to the Pan image while preserving at the same time spectral information of the MS image (Du et al., 2007). During the translation of data from the Pan to MS image, pan-sharpening methods may generate spatial and spectral distortion in the fused image. Therefore, evaluation of the quality of the fused image is required using quality metrics like qualitative and quantitative analyses.

3.7.1 Qualitative analysis

Qualitative analysis evaluates the fused image by visual interpretation; this analysis is also referred to as visual analysis. In qualitative analysis, a group of members is formed to visually evaluate the fused image by comparison with the original MS and Pan images based on various optical parameters such as spatial detail, geometric pattern, sizes of objects, and colour (Du et al., 2007). This type of analysis is a straightforward practice used to assess the quality of the fused image. However, it depends mostly on the viewing conditions and the experience of the viewer (Fonseca et al., 2011). If the viewer has excellent knowledge of the terrain in the fused image, qualitative analysis is appropriate for evaluating the quality of the fused image.

3.7.2 Quantitative analysis

Quantitative analysis is based on a mathematical model that estimates the amount of spatial and spectral distortion present in the fused image in comparison with and without reference image. In the present study, following ten quality indices were used to assess the quality of the fused image and compared the performances of the nine pan-sharpening methods.

The spectral indices such as CC (Vandermeer, 2006), Q (Alparone et al., 2004) RMSE (Zoran, 2009), SSIM (Wang et al., 2004) SNR (Alimuddin et al., 2012) and PSNR (Kumar and Singh, 2010) are used for evaluating the spectral quality of the fused image. The reference image, which is an important requirement for processing these

indices, should be an MS image with the same size as that of the Pan image. In practice, obtaining a reference image with this requirement is challenging. Nevertheless, a reference image can be obtained by resampling the original MS image to the size of the Pan image (Gangkofner et al., 2008). The spatial indices such as E (Du et al., 2007), Gradient (Wu et al., 2015) and SCC (Choi, 2006) are used for the evaluation of spatial quality with the Pan image as a reference image. The QNR (Alparone et al., 2008) indices are also used for the evaluation of spectral and spatial quality, when the ideal reference image is not available.

3.8 Quantitative indices for assessing spectral distortion

Resampling the MS image to the spatial resolution of Pan image is processed for pan-sharpening, therefore the reference MS image with the dimensions of Pan image is available for the assessment of spectral distortion (Alparone et al., 2008).

3.8.1 CC

It represents the similarity of the spectral features between the reference and fused image. The ideal value 1 is the best spectral performance of the fused image. The general mathematical form of CC is

$$CC = \frac{\sigma_{xy}}{\sigma_x \sigma y} \tag{3.3}$$

3.8.2 RMSE

Measures the spectral quality of fused image. The value 0 indicates best spectral information was retained in the fused image. The equation of RMSE is expressed as

$$RMSE = \sqrt{\frac{\sum_{i=1}^{n}(x_i - y_i)^2}{n}} \tag{3.4}$$

3.8.3 Q

Represents the amount of transformation of relevant data from the original image to the fused image. The ideal value 1 is the best spectral performance of the fused image. The mathematical form of Q is

$$Q = \frac{4\sigma_{xy} x_i y_i}{\left(\sigma_x^2 + \sigma_y^2\right)\left[x_i^2 + y_i^2\right]} \tag{3.5}$$

3.8.4 SSIM

It compares the local patterns of pixel intensities between the reference and fused images. The value 1 denotes the best fused image. The mathematical form of SSIM is

$$SSIM = \frac{(2x_i y_i + c_1)(2\sigma_x \sigma_y + c_2)}{(x_i^2 + y_i^2 + c_1)(\sigma_x^2 + \sigma_y^2 + c_2)} \tag{3.6}$$

3.8.5 PSNR

It is computed by the number of gray levels in the image divided by the corresponding pixels in the reference and the fused images. The higher PSNR value denotes the best spectral information in the fused image and it is computed using following equation

$$PSNR = 10\log_{10}\left(\frac{L^2}{\frac{1}{mn}\sum_{i=1}^{m}\sum_{j=1}^{n}(x(i,j) - y(i,j))^2}\right) \tag{3.7}$$

3.8.6 SNR

It measures the ratio between the noise and information present in the fused image. The higher SNR value indicates the best spectral information in the fused image. The following equation is used to calculate the value of SNR

$$SNR = 10\log_{10}\left(\frac{\sum_{i=1}^{m}\sum_{j=1}^{n}(x(i,j))^2}{\sum_{i=1}^{m}\sum_{j=1}^{n}(x(i,j) - y(i,j))^2}\right) \tag{3.8}$$

3.9 Quantitative indices for assessing spatial distortion

The following indices determines the spatial distortion of fused image by comparing the spatial resolution of fused and original Pan image.

3.9.1 SCC

It represents the similarity of the spatial features between the Pan and fused image. The value of SCC differs from -1 to 1. The higher value of SCC represents the best fused image with high spatial detail. The mathematical form of SCC is expressed as

$$SCC(f,y) = \frac{\sum\sum(f-\mu_f)^2(y-y_i)^2}{\sqrt{\sum(f-\mu_f)^2\sum(y-y_i)^2}} \tag{3.9}$$

3.9.2 E

It measures the information content of the fused image. The higher value of E denotes the fused image with more spatial information. The equation of E is expressed as

$$E = -\sum_{i=0}^{n-1} p(i)\ln[p(i)] \tag{3.10}$$

3.9.3 Gradient

The larger value of G denotes high gradation of the image and high spatial detail. The value of G is computed using following formula

$$G = \frac{1}{(m-1)(n-1)}\sum_{i=1}^{m}\sum_{j=1}^{n}\sqrt{\frac{1}{2}[\Delta xf(i,j)^2 + \Delta yf(i,j)^2}} \tag{3.11}$$

3.10 Quality with no reference image (QNR)

The QNR index evaluates the quality of fused image without demanding a reference image. It is efficient for assessing both the spectral D_λ and spatial D_s distortions of fused image at the full scale of Pan image. The best value of QNR is 1, which denotes that fused image contains zero spatial and spectral distortion. The mathematical equation of QNR is,

$$QNR = (1-D_\lambda)^\alpha(1-D_s)^\beta \tag{3.12}$$

where, α and β are set to one.

$$D_\lambda = \sqrt[p]{\frac{1}{n(n-1)} \sum_{i=1}^{n} \sum_{j=1, j\neq i}^{n} \left| d_{i,j}(a,y) \right|^p} \tag{3.13}$$

$$D_s = \sqrt[q]{\frac{1}{n} \sum_{i=1}^{n} \left| Q(y_i, f) - Q(a_i, f_{lp}) \right|^q} \tag{3.14}$$

where, p and q are set to one and $d_{i,j}(a,y) = Q(a_i,a_j) - Q(y_i,y_j)$.

For determining the spectral distortion, the parameter Q is calculated at both low and fused resolution, among each of the MS bands. For determining spatial distortion, the Q index is calculated between each MS bands and Pan image over both the low and high resolutions.

The inter-band computation at the two scales aid to define if there is a difference between the spectral content between MS bands across scale, thus indicating spectral distortion. The intra-band calculations at the two scales help determine the difference between the spatial information between MS bands and pan image across scale, indicating spatial distortion.

The pan-sharpening methods like PCA, M-IHS, BT, Multiplicative, W-PCA, HCS, HPF, GS and Fuze Go are adopted to fuse Pan and MS imagery of Quickbird-2 and Landsat-8. The pan-sharpened image obtained from the above mentioned pan-sharpening methods were evaluated using two approaches namely; qualitative and quantitative analyses. The input from these two analyses were considered for the selection of best pan-sharpening method which generates the image with less spatial and spectral distortion. Further, the best pan-sharpened image is adopted to the study the effectiveness of improving the spatial resolution of MS image, by extracting the buildings and by estimating the bathymetry of near-shore ocean.

3.11 Extraction of Buildings

3.11.1 General

Extraction of buildings from the satellite imageries has various significant applications in the domain of urban mapping, urban planning, urban change detection analysis, target detection and GIS. Numerous algorithms were developed for the extraction of buildings. However, majority of the algorithms work efficiently for detecting the buildings which

are in same shapes, sizes and colours.

Therefore, it is necessary to frame a methodology for the extraction of buildings which are in different sizes, shapes and colours. In order to extract the buildings; two approaches were adopted i) automatic, ii) manual as shown in the Figs. 3.10 and 3.11. However, satellite imagery with high spatial and spectral information in a single image is required to extract detail spatial and spectral information of buildings. The effectiveness of improving the spatial resolution of original MS image for the extraction of buildings were studied using automatic and manual methods.

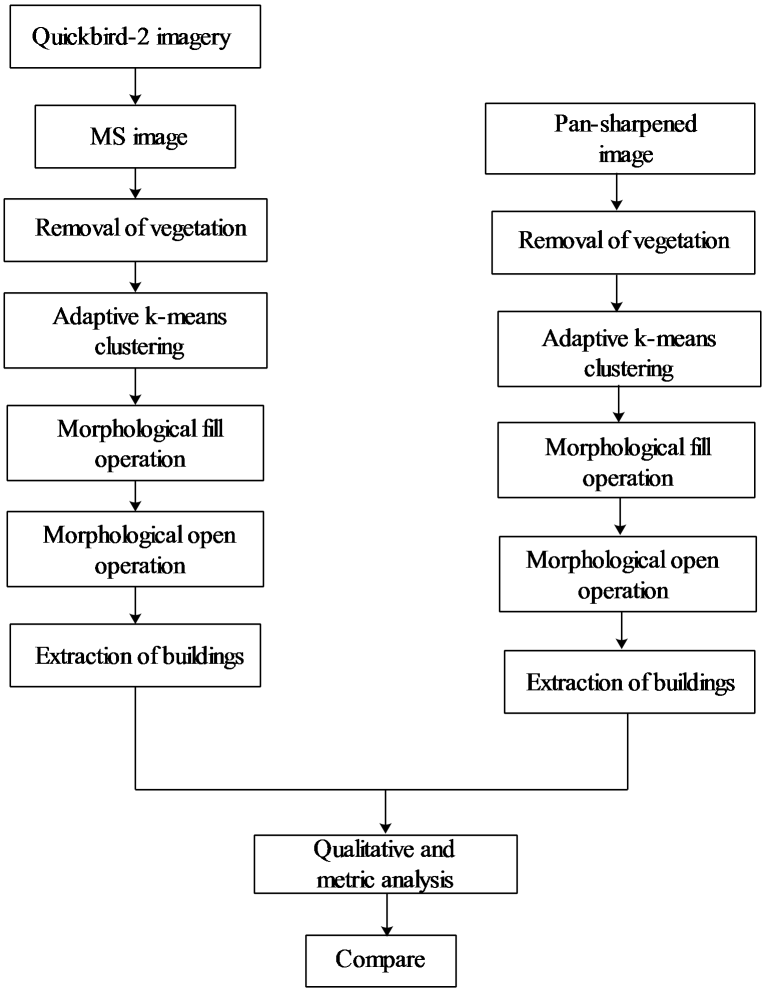

Figure 3.10 Methodology for extracting the building using automatic method

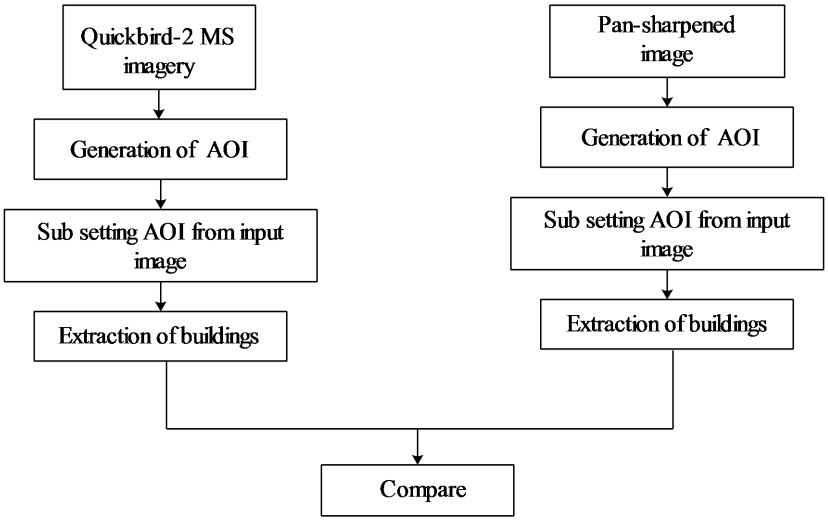

Figure 3.11 Methodology for extracting the building using manual method

3.12 Methodology for the extraction of buildings automatically

The detailed explanation of methodology for extracting the buildings automatically are explained as below, the algorithm processes automatically without pre-classification or any training sets, however some initial algorithm parameters must be set by the user.

3.12.1 Removal of vegetation portion

The multispectral image with the combination of bands B, G, R and NIR were used. From the input image in Fig. 3.2(b), it is visualised that the vegetation feature is quite dominant compared to the other features; therefore the portion of vegetation is removed based on the intensity value. The threshold value of Red > 120, Green < 100 and Blue < 100 were used for the removal of vegetation. These values need to be manually adjusted by the user.

3.12.2 Adaptive K-means clustering

The Adaptive K-means clustering algorithm functions by automatically choosing the appropriate K elements from the input image (Pappas, 1992; Chen et al., 1998). The algorithm automatically determines the K elements and generates the group of clusters (i.e. the feature with the same intensity value are grouped together). Generally, the algorithm classifies each pixel into the clusters, based on their intensity values. Firstly,

the algorithm computes the distance between the selected element and the number of clusters. This process also helps to determine the distance between the two elements.

To compute the distance, it is important to normalize the distance properties, so that the domination of distance from one property (or) certain properties are not omitted from the computation of distance. The method, euclidean distance is adequate for determining the distance between two elements. If the input data encompass n-dimension, then the distance of two elements such as $A_1 = \{A_{11}, A_{12}, \ldots, A_{1n}\}$ and $A_2 = \{A_{21}, A_{22}, \ldots, A_{2n}\}$ is given by,

$$Distance(A_1, A_2) = \sqrt{(A_{11} - A_{21})^2 + (A_{12} - A_{22})^2 + \cdots + (A_{1n} - A_{2n})^2} \qquad (3.15)$$

By the distance function, the further processing of the algorithm is denoted below: The distance is computed for each of the clusters from one another. The computed distance is warehoused in two-dimensional array as a triangular matrix. Later, the minimum distance $(d_{\min})$ among any two clusters (i.e. B_{m1} and B_{m2}) and also the two nearest clusters are identified. For any un-clustered element E_i , it computes the distance of E_i from every cluster. To assign the element E_i to the appropriate cluster, the following three different processes are mentioned.

- If the distance of the element E_i is zero from the clusters, then allocate E_i to that cluster and examine the other un-clustered elements.

- If the distance of the element E_i from the known clusters is less than the distance $(d_{\min})$ then allocate E_i to the nearest clusters. By allocating E_i to the clusters, the centroid representation of clusters may differ; therefore the centroid is recalculated for all the elements presented in the respective clusters. Further, the distance of disturbed clusters from the other clusters, minimum distance between the two clusters and the two clusters that are near to each other is also recomputed.

- If the distance $(d_{\min})$ is less than the element distance from the neighbouring clusters, then possible two nearest clusters are selected (e.g. C_{m1} and C_{m2}) then merge C_{m2} into C_{m1}. Later the elements presented in the C_{m2} cluster are removed and also the representation of respective cluster is deleted. Further, new elements are

added to the empty cluster and distance between all the clusters are re-determined and two nearest clusters are recognized again.

The above mentioned steps are iterated for all the elements to be clustered.

3.12.3 Morphological fill and open operation

3.12.3.1 Fill operation

It is used to fill the holes in the grayscale image I. A hole is defined as an area of dark pixels surrounded by lighter pixel. The following matlab syntax is used to fill holes in the image

$$I2 = imfill(I) \tag{3.16}$$

Where, I is the binary image. The advantage of fill operation is to fill the holes in the image by describing an area of dark pixels bounded by light pixels and producing another binary image $I2$.

3.12.3.2 Open operation

The morphological open operator were normally applied to the binary image. It is used to remove the features that are smaller than the value of P pixels and retains the large structure in the image.

The following matlab syntax is used to extract the objects from the input image.

$$IM = bwareaopen(I,P) \tag{3.17}$$

The open operation eliminates all the associated components (i.e. objects) that have less then P pixels from the binary image I producing another binary IM image.

3.13 Quality analysis

To evaluate the performance of automatic algorithm both qualitative and metric analysis are adopted. The following two metrics proposed by (Lin and Nevatia, 1998) were used. Here, the performance of algorithm were compared with the ground truth data which is derived manually.

$$DP = \frac{100 \times TP}{TP + TN} \tag{3.18}$$

$$BF = \frac{100 \times FP}{TP + FP} \tag{3.19}$$

Where, TP denotes the detection of buildings by both automatic algorithm and manual. FP indicates the number of buildings detected by the algorithm but not manually. TN denotes buildings extracted using a manual approach but not by the automatic algorithm. The detection of building is rated, if at least a small portion of it is detected by the automatic algorithm (Chaudhuri et al., 2016). The two metrics are computed by comparing the buildings detected by the manual approach and automatic algorithm. The metric DP calculates how many of the buildings in the image are extracted by the automatic algorithm and BF denotes how many buildings are found erroneously.

3.14 Extraction of buildings using manual method

The brief explanation of each step in the manual method is explained as below.

- Firstly, AOI is generated by drawing the polygon over the interested building on the input image.
- Secondly, the created AOI portion of the building is used to subset the buildings from the input image.

The above described approaches like automatic and manual procedures were adopted to extract the buildings from the original MS imagery of Quickbird-2 and the same procedures are adopted to extract buildings from the best Pan-sharpened image and the results of both were compared using qualitative and metric approaches.

3.15 Bathymetry Mapping

3.15.1 General

The bathymetry of ocean is surveyed using ship carrying echo sounders. Although most of the areas are unexplored due to the complications of transporting the ship to the deep ocean, estimating the bathymetry using ship is cost effective. The remote sensing based technique has advantages in comparison with the present echo sounder technique. The remote sensing satellite sensor absorbs the globe with uniform resolution and repetivity of collecting data over the same area helps to monitor changes in

the bathymetry of ocean. There are several commercially available multispectral satellite data acquired through Ikonos and Worldview, which can be used to determine the bathymetry of ocean. However, the Landsat-8 satellite imagery is available freely in the open domain. Hence, Landsat-8 imagery is utilised for determining the bathymetry of near-shore ocean. The procedure for estimating the bathymetry of near-shore ocean is shown in the Fig. 3.12.

3.16 Bathymetry from space

The Landsat -8 imagery used for the present study is downloaded from the USGS website, acquired during March 13, 2014. The Landsat-8 satellite acquires total of 11 bands including, B and G with the spatial resolution of 30 m and Pan band with the spatial resolution of 15 m. The hydrograhic chart of the study area is acquired during March 18, 2014 from NMPT, Mangaluru, India. The chart contains the sounding data, which is used against the satellite imagery as a reference data to determine the bathymetry of near-shore ocean.

The bathymetry of near-shore ocean is estimated using the B and G band pair, both the satellite imagery and hydrographic charts are co-registered correctly. The hydrographic chart represents the ground data with respect to the chart datum. The depth soundings of hydrographic chart were used to reference the satellite derived bathymetry to the chart datum. To perform the ratio transform algorithm, m_1 and m_0 values are computed from the soundings which are used as control points for the algorithm results.

During the satellite image acquisition, instant water level is very unlikely to correspond with the chart datum (e.g., MLLW (or) LAT), the measurement of tide height during the acquisition of satellite image is not needed, because it is automatically accounted for using the control points which are selected from a hydrographic chart to define the transformation parameters. Generally, the water levels over small spatial magnitude are normally well approximated as a vertical offset, and do not harm the linear relationship between the hydrographic chart soundings and the algorithm results. Thus, the procedure excludes the need for tide-corrected satellite imagery and for tide correctors (Pe'eri et al., 2014).

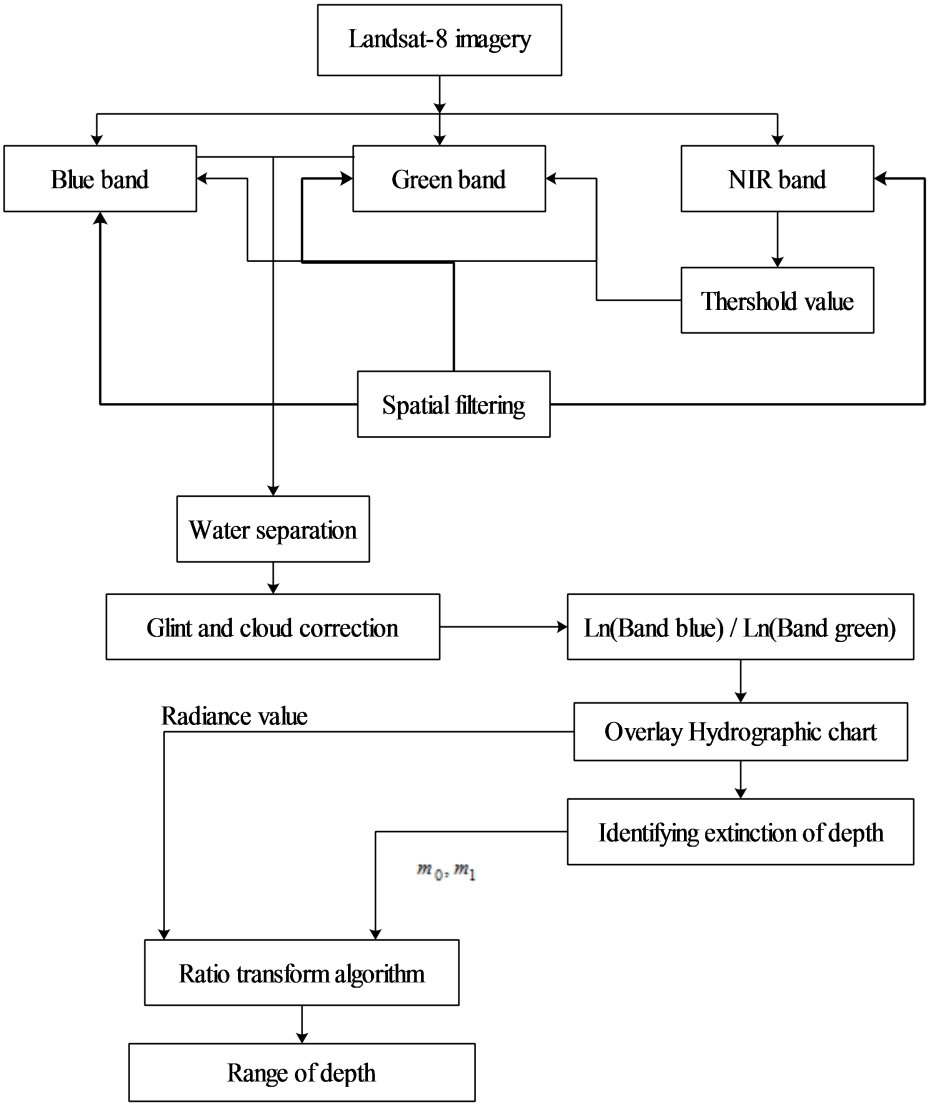

Figure 3.12 Methodology for estimating the bathymetry of near-shore ocean

The detailed explanation of methodology for estimating the bathymetry of near-shore ocean is described as below;

3.16.1 Spatial filtering

During the acquisition of image, sensors in the orbit may generate the speckle noise. The primary cause for the speckle noise is the interference of the reflectance energy at the transducer aperture. Therefore, it is important to pre-process the B, G and NIR bands of landsat-8 imagery to remove the speckle noise. A spatial filtering technique called low pass filter (kernel size 5x5) is applied on the B, G and NIR bands of Landsat-

8 imagery to remove the speckle noise. The low pass frequency components denotes smooth (water) regions, therefore low pass-filter is appropriate to remove the speckle noise.

3.16.2 Water separation

It is important to separate land from water to estimate the bathymetry of ocean. For this purpose, NIR band is used due to the appearance of water in dark and land in bright. Here, the land/water threshold value is obtained by drawing a line that crosses from land (bright areas) into the water (dark areas). The obtained threshold value is applied on the B and G band of Landsat-8 imagery to separate land from water.

3.16.3 Glint and cloud correction

This step is intended to correct the radiometric contribution from sun glint and low clouds; the method proposed by (Hedley et al., 2005) is performed to rectify the radiometric correction on the B and G bands. The linear relationship between the NIR and visible bands (i.e. G and B) is established using the linear regression, based on a selected sample area of the image pixels. Following the recommendation of (Hochberg et al., 2003) sample region of image is selected which is evident of sun glint, but the spectral brightness of the selected region is expected to be consistent, wherein the region of deep water is ultimate for this. The equation for removing the sun glint and low clouds is shown below.

$$R_i' = R_i - b_i(R_{NIR} - Min_{NIR}) \tag{3.20}$$

Where, R_i is the pixel value in B and G band, b_i is the regression slope, $R_{NIR} - Min_{NIR}$ is the difference between the pixel NIR value of R_{NIR} and the ambient NIR level Min_{NIR} which gives the R_i' sun glint corrected pixel brightness in the band B and G. The value of Min_{NIR} indicates the pixel brightness of NIR with no sun glint, and can be assessed by the minimum NIR value, which is found in the regression sample. Generally, the minimum NIR pixel is less prone to problematic outliers than the maximum NIR pixel. The following steps are implemented to remove the radiometric correction on B and G bands.

- Select the sample area where the range of sun glint is evident. It is important to note that the image might be more or less homogeneous, if the sun glint was not present (in deep water) and estimate the Min_{NIR} in the sample.

- To remove the sun glint from the $band_i(band_{blue}, band_{green})$, perform the linear regression by using the selected pixels of NIR brightness (x-axis) against $band_i$ (y-axis). And determine the slope of the regression line for the $band_i$, which is denoted as b_i .

- To remove the sun glint from the $band_i$ (for all pixels in the image), subtract the outcome of b_i and the NIR brightness of the pixel minus Min_{NIR} from the pixel value in the $band_i$.

3.16.4 Ratio transform algorithm

The ratio transform algorithm was proposed by (Stumpf et al., 2003), is used to estimate the bathymetry of near-shore ocean. The algorithm makes use of two bands in order to reduce the number of parameters to infer the depth of the ocean. It decreases the bottom most radiance of one band more rapidly with respect to depth, when compared to another band. This leads to the ratio between the two bands to differ with respect to the depth. A near constant attenuation value will be preserved between the ratio of two bands which is nothing but the difference of the diffuse attenuation coefficient at two different wavelengths; just depending on notion that water column is uniformly mixed.

The algorithm can cut down the error coupled with varying radiation in the atmosphere, water column and sea floor, for the reason that both bands are distributed equally. Typically in the coastal environment, radiance in the blue wavelength (400-500 nm) attenuates faster with depth, than light in the green wavelength (500-600 nm). Thus, the variation in ratio between the bands is affected further by the depth than by bottom reflectance. To infer the bathymetry, the algorithm establishes the linear relationship between the ratio of radiance in two bands (G, B) and water depth.

The algorithm relays on the circumstance that the absorptivity of water differs spectrally from band to band. As the depth of water increases, reflectance values of the band with higher absorption will decrease proportionately faster than reflectance value

of the band with lower absorption. Therefore, when two bands are transformed, it exist a linear decrease between a ratio of high absorption band to a low absorption band and water depth.

The following equation is used to determine the depth of the near-shore ocean:-

$$z = m_1 \left(\frac{\ln(L_{obs}(Band_i))}{\ln(L_{obs}(Band_j))} \right) - m_0 \tag{3.21}$$

Where, m_1 and m_0 are determined empirically. The advantage of ratio transform algorithm is that, it takes very few parameters and does not require any optical properties to determine the depth of ocean.

3.16.5 Identifying the extinction depth

The statistical analysis R^2 is adopted to estimate the extinction of depth. The R^2 closest to 1 indicates that there exists a linear relationship between the satellite derived bathymetry and the reference hydrographic chart datum. Here, the reference hydrographic chart is overlaid on the output of $\ln(L_{obs}(Band_{blue}))/\ln(L_{obs}(Band_{green}))$ and the corresponding pixel value from the satellite image and corresponding hydrographic chart value is obtained to determine the extinction of depth. The region deeper than the extinction depth do not match the algorithm results with the reference hydrographic chart, therefore the value of R^2 does not show clear correlation. The parameters such as m_1 and m_0 are obtained from the analysis of coefficient of determination and they are further fine tuned to match the algorithm result.

Finally, the calculated parameter such as observed radiance of band from the ratio of band B and G, the value of m_1 and m_0 are provided as input to the ratio transform algorithm and identified the depth along the near-shore ocean of Mangaluru coast, Karnataka. The following statistical indices like RMSE and MAE are used to evaluate the performance of ratio transform algorithm.

$$RMSE = \sqrt{\frac{\sum_{i=1}^{n}(r_i - t_i)^2}{n}} \tag{3.22}$$

$$MAE = \frac{\sum_{i=1}^{n}|r_i - t_i|}{n} \tag{3.23}$$

The procedure for estimating the bathymetry are processed using the ArcGIS 10.2 environment. The same procedure is adopted on before and after improving the spatial resolution and the results of both were compared using statistical indices.

The study focuses on improving the spatial resolution of multispectral imagery of Quickbird-2 and Landsat-8 using nine different pan-sharpening methods. The inputs obtained from the qualitative and quantitative analysis were considered for selecting the best pan-sharpening method. The effectiveness of improving the spatial resolution of Quickbird-2 imagery is studied by extracting the buildings from the best pan-sharpened and original MS images. Further, the effectiveness of improving the spatial resolution of Landsat-8 imagery is studied by estimating the bathymetry of near-shore ocean using best pan-sharpened and original MS images.

Chapter 4

RESULTS AND DISCUSSION

4.1 General

The work comprises of four objectives that have been designed. They are: to improve the spatial resolution of multispectral imagery of Quickbird-2 and Landsat-8 using nine pan-sharpening techniques to overcome the constrains of satellite sensors, to explore an efficient pan-sharpening method using qualitative and quantitative analysis. Furthermore, the best pan-sharpened image is then selected and employed for the extraction of buildings from the Quickbird-2 imagery, and for estimating the bathymetry of near-shore ocean using Landsat-8 imagery. The results indicate that, the best pan-sharpened image can be used for remote sensing applications studies which demands both high spatial and rich spectral information in a image. The deliverables of the study are presented in three sections below:

4.2 Pan-sharpening the multispectral imagery of Quickbird-2 and Landsat-8 and quality evaluation using qualitative and quantitative analysis

The Quickbird-2 and Landsat-8 satellite sensors acquires images of earth surface in two modes like Pan and MS. The Pan image have high spatial information, whereas MS image have rich spectral information but low spatial resolution. The remote sensing applications requires both the qualities in a single image. Therefore, nine different pan-sharpening techniques were adopted to improve the spatial resolution of multispectral imagery of Quickbird-2 and Landsat-8. To evaluate the quality of these pan-sharpening techniques both qualitative and quantitative analysis were performed and compared for

the selection of best pan-sharpening technique. The results obtained from the different pan-sharpening techniques and their quality evaluation using qualitative and quantitative approaches are presented and discussed as below.

The image size of landsat-8 is 170 km x 185 km and image size of Quickbird-2 is 16.5 km x 16.5 km. Since the size of the images is large, it was not promising to compare visually every individual feature; therefore subset images were presented to highlight the effect of nine pan-sharpening methods.

The original Quickbird-2 MS images with the band combination of R, G, B, and NIR in addition to the Pan image are displayed in Figs. 3.2(a) and 3.2(b). The original MS image was resampled to the size of the Pan image is shown in Fig. 3.2(c). The fused results of Quickbird-2 imagery attained from the nine different pan-sharpening methods are presented in Figs. 4.1(a) - 4.1(i).

The original MS image with the combined R, B, and G bands in addition to the Pan image of Landsat-8 are shown in Figs. 3.3(a) and 3.3(b). The resampled MS image to the size of the Pan image is shown in Fig. 3.3(c). All of the Landsat-8 fused images obtained by the nine different pan-sharpening methods are presented in Figs. 4.2(a) - 4.2(i).

4.2.1 Qualitative analysis

All of the pan-sharpened images and the original MS image of Landsat-8 imagery are displayed in the RGB color mode as bands 1, 2 and 3 for each respective color. Those of Quickbird-2 are displayed in the RGB color mode as bands 4, 3 and 2 also for each respective color. For reasonable assessment and comparison of the quality of the pan-sharpened images, all of the pan-sharpened, MS, and Pan images of Quickbird-2 and Landsat-8 are displayed at the same zoom level. A group of eight remote sensing experts (with Master's qualification in remote sensing and GIS) was engaged to evaluate the quality of the pan-sharpened images based on improvement in the spatial information, preservation of the spectral information, and spatial and spectral distortion. The inputs obtained from the experts is shown in the Table 4.1 (best fused image are shown in bold) were considered in the ranking of pan-sharpening methods. Generally, all of the pan-sharpening methods increased the spatial detail of the MS image to that of the Pan

image. Furthermore, small features that were not noticeable in the original MS image were identified in the pan-sharpened image.

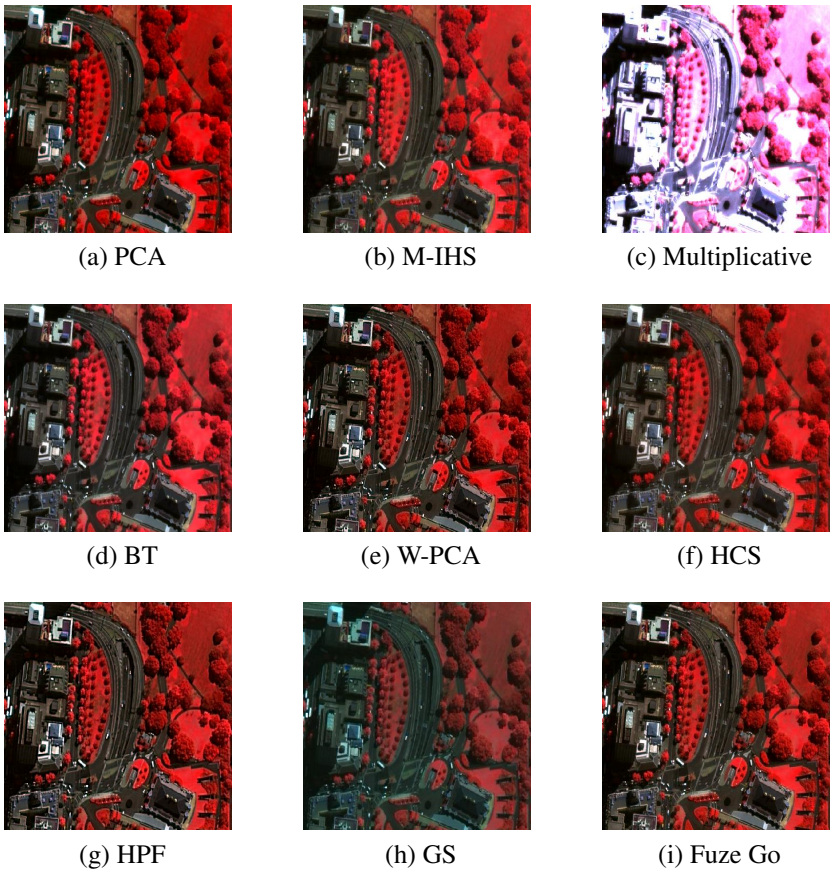

(a) PCA (b) M-IHS (c) Multiplicative

(d) BT (e) W-PCA (f) HCS

(g) HPF (h) GS (i) Fuze Go

Figure 4.1 Quickbird-2 pan-sharpened image

The pan-sharpened images obtained using the PCA method are shown in Figs. 4.1(a) and 4.2(a). The spatial information was improved, and the PCA generated minor color variations in the fused image. The pan-sharpened images generated by the M-IHS method, presented in Figs. 4.1(b) and 4.2(b), preserved the color information and rendered better spatial details similar to the original MS and Pan image. The results of multiplicative fused images are presented in Figs. 4.1(c) and 4.2(c). This method failed to generate a satisfactory fused image because the spectral details and spatial information were not preserved. The pan-sharpened image of the multiplicative method contained more spectral and spatial distortion, which is differs significantly from the

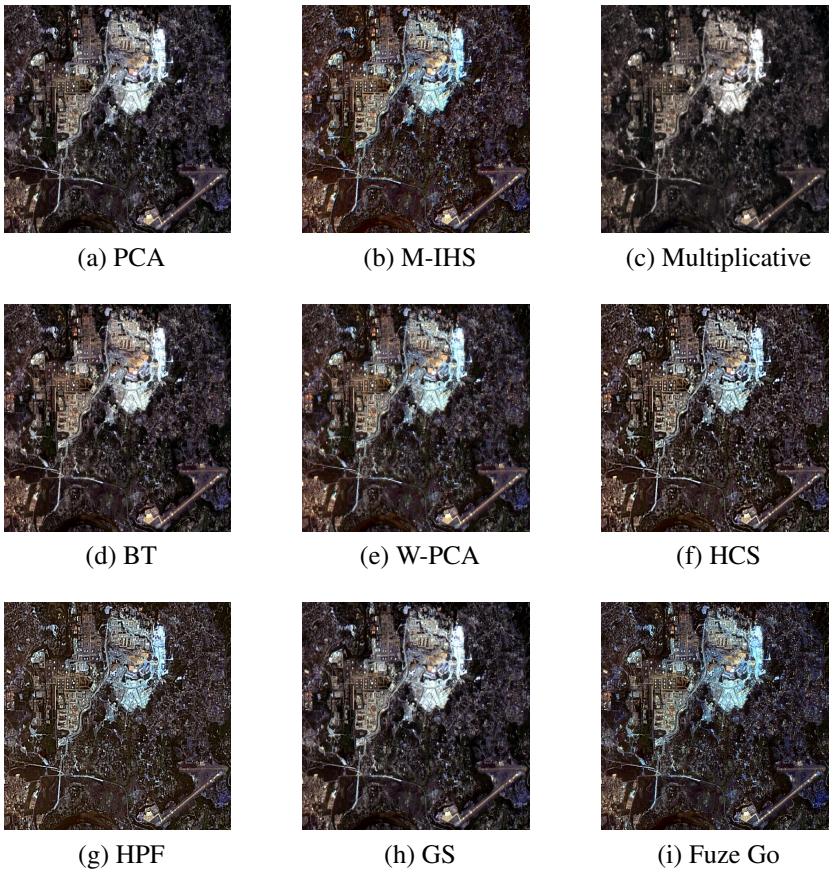

(a) PCA (b) M-IHS (c) Multiplicative

(d) BT (e) W-PCA (f) HCS

(g) HPF (h) GS (i) Fuze Go

Figure 4.2 Landsat-8 pan-sharpened image

original MS and Pan images. The BT pan-sharpened images, shown in Figs. 4.1(d) and 4.2(d), best preserved the spectral information and increased the contrast, which resulted in visually appealing image.

Among the PCA, BT, M-IHS, and multiplicative pan-sharpened images, the PCA and BT methods were similar. The BT method is superior to PCA because it preserved the color information, whereas M-IHS performed slightly better than the PCA, BT and multiplicative methods.

In the pan-sharpened images produced by the W-PCA method, as shown in Figs. 4.1(e) and 4.2(e), improvement was noted in the spatial information. Moreover, the spectral information retained was nearly identical to the original MS image. The pan-sharpened images obtained using HCS method, presented in Figs. 4.1(f) and 4.2(f), preserved the spectral information. However, fewer spatial details were retained compared with those in the original Pan image such that small features were unable to be

identified. The HPF fused images, shown in Figs. 4.1(g) and 4.2(g), exhibit high spatial details, and the spectral information was preserved. The pan-sharpened images obtained by the GS method, displayed in Figs. 4.1(h) and 4.2(h), best preserved the color intensity, although the borders of the features were not as sharp.

The pan-sharpened images obtained using W-PCA, HPF, and GS methods appear to be similar. However, the color intensity of the W-PCA images is marginally weaker than that in the HPF and GS methods. The HPF method performed slightly better than the W-PCA and GS methods.

The pan-sharpened images obtained by the Fuze Go method, shown in Figs. 4.1(i) and 4.2(i), contain high spatial details and preserved spectral information. Because it produces a sharper pixel size and preserves the spectral information in the fused image, this method has an advantage of enabling the identification and differentiation of small features spatially and spectrally. Moreover, this method generates images that match the spatial details of Pan image and the color information of MS image.

In comparison with other methods such as HPF, GS, M-IHS, and W-PCA, the Fuze Go method performed better by improving the spatial detail and by preserving the color information. In the qualitative analysis, the Fuze Go processed image was ranked first by five of the remote sensing experts. The HPF-processed image was ranked first by three experts, and the GS method was ranked second by three experts. It is concluded that the Fuze Go method is superior, followed by the HPF and GS methods.

4.2.2 Quantitative analysis

To validate the results of qualitative analysis, the spatial and spectral indices were used to assess the quality of Quickbird-2 and Landsat-8 fused images. These indices require the following conditions to be satisfied for selecting the best fused image with high spatial details and spectral information: i) SCC, CC, Q, QNR and SSIM should be close to one; ii) RMSE should be close to zero; iii) E, PSNR, SNR and Gradient should have a higher value.

The results obtained from ten statistical indices are shown in the Tables 4.2 - 4.7. The bold value in the tables shows best fused image. Tables 4.2 and 4.3 represent the

Table 4.1 Ranking of different fusion methods by remote sensing experts

Fusion methods \ Experts	A	B	C	D	E	F	G	H
Fuze Go	2	**1**	2	**1**	**1**	2	**1**	**1**
PCA	6	8	7	7	6	7	8	8
M-IHS	5	7	6	8	7	4	6	5
BT	8	5	8	4	5	6	7	4
W-PCA	4	4	3	5	4	5	4	6
HPF	**1**	2	**1**	3	2	**1**	3	3
GS	3	3	4	2	3	3	2	2
HCS	7	6	5	6	8	8	5	7
M	9	9	9	9	9	9	9	9

results of spatial indices such as SCC, Gradient and Entropy obtained for Quickbird-2 and Landsat-8 imagery.

Table 4.2 Spatial indices comparison between different fusion methods for Quickbird-2 imagery

Parameter \ Fusion methods	Fuze Go	PCA	M-HIS	BT	W-PCA	HPF	GS	HCS	M
SCC	**0.9113**	0.6591	0.7083	0.6076	0.7329	0.8895	0.7453	0.7229	0.5367
Gradient	**5.5737**	3.5317	3.9222	3.8177	4.8269	5.0191	4.9807	3.1271	1.0489
E	7.1288	2.9177	2.7031	2.5449	5.6749	**7.5436**	5.8037	3.9769	1.2348

Table 4.3 Spatial indices comparison between different fusion methods for Landsat-8 imagery

Parameter \ Fusion methods	Fuze Go	PCA	M-HIS	BT	W-PCA	HPF	GS	HCS	M
SCC	**0.9359**	0.7276	0.7680	0.6516	0.8206	0.8753	0.7860	0.6829	0.5106
Gradient	**8.7132**	4.5047	5.2222	4.6720	6.7169	7.1158	6.9807	4.1146	2.9987
E	6.1288	4.8177	4.7031	3.5449	5.5749	**6.3126**	5.8037	4.0769	0.2348

Here the value of SCC and Gradient indicates that the method Fuze Go produced the fused image with less spatial distortion, therefore best preserved the spatial details followed by HPF and GS. The value of entropy ranges from 0.2-7.5 approximately;

the highest value of 7.54 and 6.31 for Quickbird-2 and Landsat -8 images has been attained in the HPF fused image, consequently the method produced image with less spatial distortion. It is also notable that the method multiplicative was ranked last for all the spatial indices and hence this method generated fused image with high spatial and spectral distortion.

Table 4.4 Spectral indices comparison between different fusion methods for Quickbird-2 imagery

Parameter / Fusion methods	CC	RMSE	Q	SSIM	PSNR	SNR
Fuze Go	**0.9611**	**1.6351**	0.7215	**0.9525**	37.8464	**28.4753**
PCA	0.6591	2.8454	0.4825	0.5191	26.6675	21.0095
M-IHS	0.6482	2.9212	0.4939	0.5221	25.1466	19.0125
BT	0.5076	3.2092	0.3594	0.4048	19.1225	16.7299
W-PCA	0.7895	2.0881	0.6207	0.7719	34.4284	19.8285
HPF	0.8253	1.8512	0.6746	0.8971	**39.2962**	26.0784
GS	0.8029	1.9804	**0.8140**	0.8639	35.2943	25.1253
HCS	0.6367	2.6126	0.5868	0.6303	28.4325	20.9784
M	0.5061	6.8153	0.2167	0.0801	15.4581	12.5013

Table 4.5 Spectral indices comparison between different fusion methods for Landsat-8 imagery

Parameter / Fusion methods	CC	RMSE	Q	SSIM	PSNR	SNR
Fuze Go	**0.8359**	**1.7641**	0.7615	**0.9475**	29.8652	**23.4172**
PCA	0.6276	2.9524	0.5382	0.6966	19.7685	19.3511
M-HIS	0.6680	3.4715	0.5639	0.6821	20.5256	18.0379
BT	0.6216	3.6398	0.4294	0.5126	12.0824	14.8724
W-PCA	0.7453	2.6531	0.6907	0.7531	27.7991	19.4603
HPF	0.7860	1.9026	0.7146	0.8354	**30.2962**	21.1372
GS	0.7229	2.1298	**0.8940**	0.7739	26.2943	20.6510
HCS	0.6906	2.9173	0.5868	0.7525	24.0478	18.1047
M	0.4619	8.0512	0.3812	0.1825	15.0824	11.3721

Table 4.6 Evaluation of different fusion methods using QNR indices for Qucikbird-2 imagery

Parameter \ Fusion methods	Fuze Go	PCA	M-IHS	BT	W-PCA	HPF	GS	HCS	M
QNR	**0.9177**	0.5595	0.5978	0.5871	0.7835	0.8598	0.8121	0.7025	0.3274

Table 4.7 Evaluation of different fusion methods using QNR indices for landsat-8 imagery

Parameter \ Fusion methods	Fuze Go	PCA	M-HIS	BT	W-PCA	HPF	GS	HCS	M
QNR	**0.8930**	0.6037	0.6354	0.5702	0.7537	0.8440	0.8247	0.7144	0.3106

Spectral indices like CC, RMSE, Q, SSIM, PSNR and SNR obtained for Quickbird-2 and landsat-8 imagery are shown in the Tables 4.4 and 4.5. From the value of CC, RMSE, SSIM and SNR, it is observed that the fused image produced by the Fuze Go method best preserves the spectral information followed by HPF and GS methods. The Q index value indicates that the value of GS method was very close to the original value of Q followed by Fuze Go and HPF methods; therefore, the GS retained the maximum spectral information in the fused image similar to the original MS image. For PSNR, the highest value was obtained by HPF followed by Fuze Go and GS. The index values of Fuze Go and HPF varied about by 1. However, the merged image obtained by the HPF method contained less noise and more spectral information.

Tables 4.6 and 4.7 represents the result of QNR obtained for Quickbird-2 and landsat-8 imagery. The statistical value of QNR indicates that the index value of the Fuze Go method is superior, followed by HPF and GS methods. In comparison with other methods, the Fuze Go method is efficient for generating a fused image with high spatial and spectral quality.

Overall, the results of the three spatial quantitative analyses revealed that the Fuze Go method was ranked first of the two statistical indices like SCC and Gradient. Therefore, Fuze Go method best enhanced the spatial resolution of MS image followed by HPF method. The result of the six spectral quantitative analyses revealed that the Fuze Go method was ranked first of the four indices like CC, RMSE, SSIM, and SNR,

whereas the HPF method ranked first by PSNR. The method GS was ranked first by Q. Therefore, the Fuze Go method best preserves the spectral information of the pan-sharpened image followed by HPF and GS methods.

4.3 Differences between Fuze Go and other algorithms

The pan-sharpening algorithm such as PCA, IHS, BT, Wavelet and HPF are developed based on the assumption that, the grey value data of Pan and MS images are similar. Therefore, fused images can be attained by extracting high spatial resolution information from the Pan image and then adding it into all bands of the MS image.

Numerous other pan-sharpening algorithms including GS and modified algorithms assume that the image difference affected by seasonal and regional, differences does not impact the quality of image unless the sensor differences are considered. Therefore, one set of fusion parameters that are effective for some images of a specified sensor can be applied to the fusion of all images of the sensor, without considering spectral differences caused by seasonal and regional differences.

However, the pan-sharpening algorithm processed by these assumption will attain good fusion results for some images, but fails with other images. On the contrary, Fuze Go algorithm treats each set of Pan and MS images separately to find out the finest fit between the Pan and MS images and then fuse them together. Therefore, it constantly achieves good fusion results regardless of the differences in sensors, seasons, and regions.

The spatial resolution of multispectral imagery of Quickbird-2 and Landsat-8 was improved using different pan-sharpening techniques, the quality of these pan-sharpening techniques was evaluated using qualitative and quantitative analysis. The results of these analyses revealed that the fused image generated by the Fuze Go method best enhanced the spatial details and preserved the spectral information. Therefore the fused image of Fuze Go method is further employed for the extraction of buildings from the Quickbird-2 imagery and for estimating the bathymetry of near-shore ocean using Landsat-8 imagery.

4.4 Extraction of buildings

The buildings from the original mutlispectral imagery of Quickbird-2 were extracted using automatic and manual approach. In the automatic approach; firstly, the vegetation portion was removed from the input image. Secondly, adaptive k-means clustering algorithm was adopted to cluster the pixels into different classes. Finally, the morphological fill and open operator was implemented to extract the buildings. In the manual approach, AOI was created from the input image. Later, the generated AOI was used to subset the interested features (i.e. buildings) from the image. Further, to study the effectiveness of improving the spatial resolution of multispectral imagery, the same procedure is adopted on the pan-sharpened image generated by the Fuze Go method and the results of both were compared using qualitative and quantitative approaches are presented and discussed as below.

The original Pan and MS images are shown in the Figure 3.3(a) and 3.3(b). The original MS with the combination of band B, G, R and NIR contains different features like buildings, roads, vehicles and vegetation etc. It is important to note that the pattern, shape, size and spectral reflectance of the buildings vary from each other. It is also visualized that the color reflectance of roads and color reflectance of buildings are similar. Therefore, the attempt is made to extract the buildings with different size, shape, color and pattern.

The automatic approach for extracting the buildings from the original MS image is shown in Fig. 4.3. Firstly, the vegetative portion of the image is removed based on the intensity value and shown in Fig. 4.3(a). The threshold value of red > 120, green < 100 and blue < 100 were used for the removal of vegetation. These values need to be manually adjusted by the user. In this experiment, the above mentioned values are found to give satisfactory results for the removal of vegetation. Secondly, the adaptive k-means clustering algorithm automatically classifies the different pixels based on the intensity value into five different classes as shown in the Fig. 4.3(b), and here the majority of buildings were observed in the class two. It is further observed that only the roof tops coming under class four and five appear comparatively brighter. Majority of building portion comes under the class two, therefore, the pixels coming

under the class four and five were removed to extract the majority of buildings. From the classified image, it is notable that the buildings with the same intensity value are clustered into one class. Further, it is also noted that the intensity value corresponding to some buildings is close to the intensity value of roads and hence it is segregated in the same class.

(a) Removal of vegetation

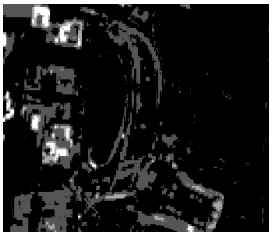

(b) Adaptive k-means clustering

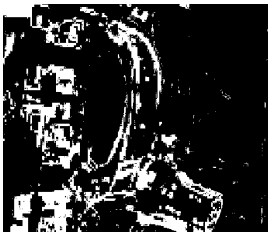

(c) Conversion of classified image into binary image

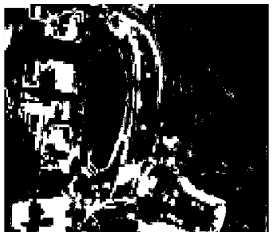

(d) Morphological fill operation

(e) Morphological area open operation

(f) Conversion of binary image (area open) to RGB

Figure 4.3 Automatic approach for the extraction of buildings using original MS image of Quickbird-2

Majority of buildings were found only in class two. Therefore the binary image is created only for the class two and is shown in the Fig. 4.3(c), the small portion of buildings which are presented in other classes were ignored. It clearly indicates that some portion of the road is identified as building due to the similarity in intensity value and spectral reflectance. The same behaviour is noticed in literature (Ghaffarian and Ghaffarian, 2014; Liasis and Stavrou, 2016). However, the morphological fill operation helps in restoring some of these pixels which were lost in the above process. Since some buildings roof top are void, in order to reduce the potential error, the voids were filled using morphological fill operator (i.e. the void presented in the buildings, after the classification process is identified with the reference to the original pan image) which is

shown in Fig. 4.3(d). To extract the buildings from the image, the morphological area open operator is adopted and the result is shown in Fig. 4.3(e). The extracted buildings in the RGB color mode is shown in Fig. 4.3(f).

To determine the effectiveness of improving the spatial resolution of the original MS image. The same methodology of automatic approach for the extraction of buildings were adopted on the Fuze Go pan-sharpened image and shown in the Fig. 4.4. The removal of vegetation portion is shown in Fig. 4.4(a). The classification of different features using adaptive k-means clustering is shown in Fig. 4.4(b). Consequently, conversion of classified image into the binary image followed by morphological fill and open operation are shown in Figs. 4.4(c), (d) and (e). The extraction of building in the RGB color mode is shown in the Fig. 4.4(f).

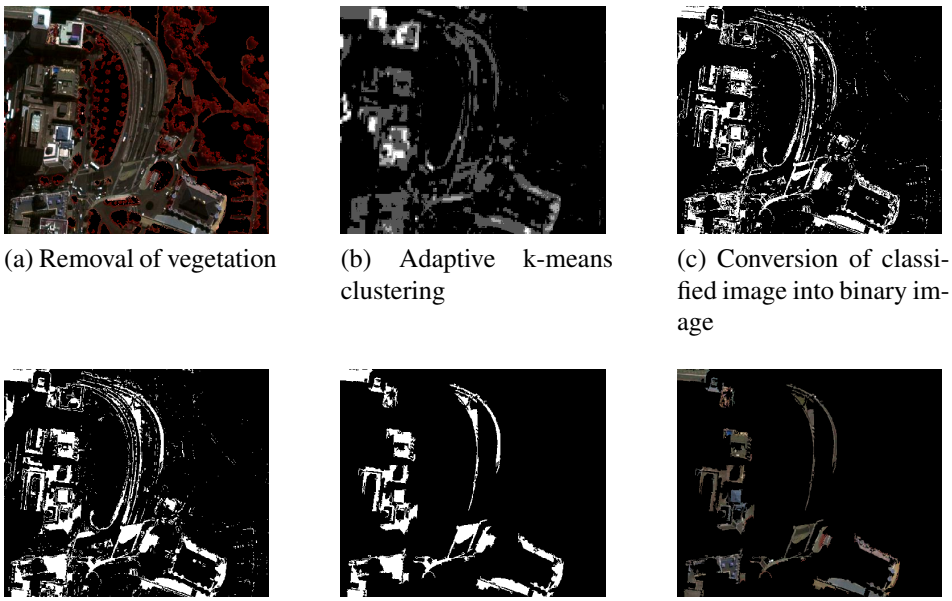

(a) Removal of vegetation

(b) Adaptive k-means clustering

(c) Conversion of classified image into binary image

(d) Morphological fill operation

(e) Morphological area open operation

(f) Conversion of binary image (area open) to RGB

Figure 4.4 Automatic approach for the extraction of buildings using pan-sharpened image

To evaluate the performance of automatic algorithm both metrics and visual analysis were used. The total number of buildings presented in the input image is twelve. The performance of automatic algorithm using two metrics like DP and EF is shown in the Table 4.8. Here, the building detection percentage of automatic algorithm for before

fusion image and after fusion image were reasonable for such a challenging MS image. However, the branch factor indicates the percentage of buildings found erroneously. It is notable that some portion of the road is identified as buildings due to the similarity in intensity value and spectral reflectance. However, the loss of information is higher in pan-sharpened image compared to the original image. The consequence of the spatial resolution of image for detecting the buildings are presented in (Segl and Kaufmann, 2001). The common challenge for detecting buildings from less than or equal to 1m pixel resolutions are low-signal to noise ratio and weak objects signal.

Generally, it is well understood that the loss of information is evident for the extraction of buildings using any automatic algorithm. The loss of information may be higher or lower which is totally dependent on the scene complexity, building variability and abundance in the urban areas. If there exists a significant difference in the feature size, pattern and shape, loss of information ensues. In our case, majority of buildings were found in the class two. Therefore, the binary image is created only for the class two, and the small portion of buildings which are presented in other classes were ignored. However, the morphological fill operation helps in restoring some of these pixels which were lost in the above process. If the threshold value for morphological open operation is too large or small, it may lead to over and under segmentation respectively.

Table 4.8 Evaluation of automatic algorithm using two metrics DP and BF.

Image	TP	FP	TN	DP(%)	BF(%)
Original MS	09	03	03	75	25
Pan-sharpened	08	04	04	66.6	33.3

The visual comparison of spatial and spectral information of extracted buildings from the automatic approach (i.e. before fusion and after fusion) are shown in Fig. 4.5. Here, the circle indicates the sample location to differentiate the extracted buildings in terms of spatial and spectral information.

The circles A, B and C represent the sample extraction of building which differ in pattern, color, size and shape. In the circle A of Fig. 4.5(b), a small white portion on top

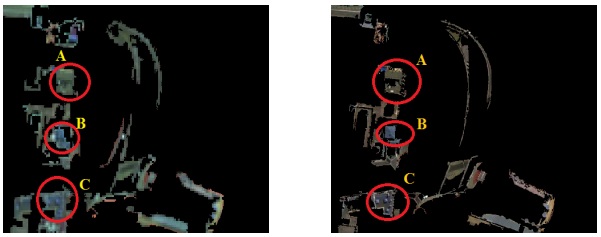

(a) Extraction of buildings from the original MS imagery of Quickbird-2

(b) Extraction of buildings from the pan-sharpened image

Figure 4.5 Qualitative analysis for the extraction of buildings using automatic approach

of the building is clearly visible both spatially and spectrally, whereas the same object is not clearly visible in Fig. 4.5(a). The circle B of Fig. 4.5(b), representing the rooftop of the building is clearly interpreted both spatially and spectrally, when compared to circle B in Fig. 4.5(a). Moreover, the circle C in Fig. 4.5(b) indicates that the building roof top with tiny structures, is clearly visible in size, shape and color, whereas the same tiny structures are not identified in Fig. 4.5(a).

Therefore, it is evident that the improvement in the spatial and spectral information helps to determine the information of buildings more effectively. However, loss of information is visible in both the images due to various factors such as pattern, size, shape and color of buildings which are different from each other and some of the buildings having same color reflectance as a road. Moreover, detailed spatial and spectral information about buildings are high in the pan-sharpened image when compared to the original MS image.

In order to extract the buildings without any loss of information, the manual extraction method is adopted using ERDAS imagine 2014 software. At first, area of interest (AOI) was created with the interested features (i.e. buildings) in the input image. Secondly, the same AOI is used to subset the interested features from the image. The same methodology adopted to extract the buildings from the original MS image and the pan-sharpened image are shown in Fig. 4.6. Here, the manual method extracts all the buildings without any loss of information. The pan-sharpened image with high spatial and spectral information helps to extract the buildings information effectively. Never-

theless, manual extraction of building is time consuming and also depends on the user experience to digitize the boundary of buildings for effective extraction of buildings.

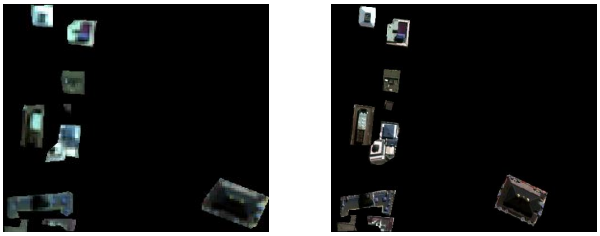

(a) original MS imagery (b) Pan-sharpened image

Figure 4.6 Manual approach for the extraction of buildings using original MS image and pan-sharpened image

By comparing the results of both automatic and manual methods, it is understandable that the automatic algorithm works efficiently when the interested features in the image are recognized to be in the same pattern and size. Generally, the loss of information is common regardless of input image (i.e. features with the same size or different size, same shape or different shape and same pattern or different pattern). Here, the loss of information in the automatic algorithm is noted for various reasons like different building size, shape, pattern and color. In the case of manual method, the loss of information for extracting buildings is less, but the method requires more time to complete the process.

4.5 Estimation of Bathymetry

The procedure based on the ratio transform algorithm is adopted to estimate the bathymetry of near-shore ocean along the coast of Mangaluru, India using Landsat-8 imagery, and the same procedure is adopted on the Fuze Go pan-sharpened image. The results of both original and pan-sharpened image were compared using statistical indices like RMSE and MAE. The obtained results from both the images are presented and discussed as below.

For this study, B, G and NIR bands of Landsat-8 imagery are used. The spatial resolution of band B, G and NIR is 30 m. The reason for applying the B and G band in the coastal environment is that radiance in the B band (450- 515 nm) decreases more rapidly

with depth than radiance in the G band (525-600 nm). Generally, light at wavelengths above 700 nm has a very low transmittance in sea water. Therefore, water appears dark and the land appears bright. For this reason, the NIR band (845-885 nm) is used for distinguishing water from land. Figs. 4.7(a), (b) and (c) represents the B, G and NIR bands of Landsat-8 satellite imagery.

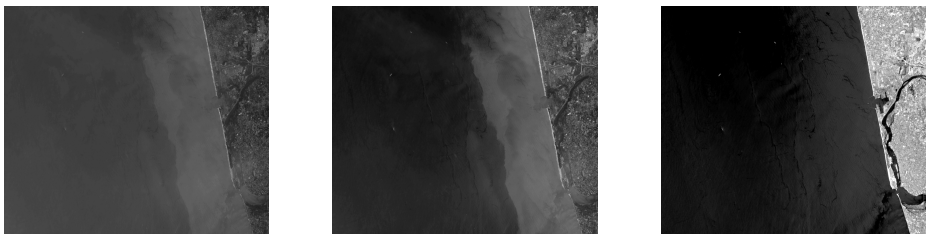

(a) B band (b) G band (c) NIR band

Figure 4.7 B, G and NIR bands of Landsat-8 imagery

To estimate the bathymetry of near-shore ocean, a procedure based on ratio-transform was adopted using the Landsat-8 satellite imagery. The results of the procedure implemented are presented in Figs. 4.8 to 4.17. It is important to pre-process the satellite image before estimating the bathymetry of near-shore ocean. Therefore, the low-pass filter is applied on the band B, G and NIR as shown in Figs. 4.8(a), (b) and (c) respectively. To separate the land from water, the threshold value estimated from the band NIR is shown in Fig. 4.9, which indicates the smooth section with low values representing water, whereas the fluctuating high values represent land. Thus, the threshold value 7000 is applied on the band B and G to separate the water from land as shown in Figs. 4.10(a) and (b).

To remove the silver glint, (Hedley et al., 2005) method is adopted. First, the polygon is drawn which covers only the water area (from the recommendations of (Hochberg et al., 2003), areas of deep water ideal for this). The polygon is created over the NIR band. The extracted polygon covers only the water area is next used to extract the water body of the B and G bands and shown in Figs. 4.11(a) and (b).

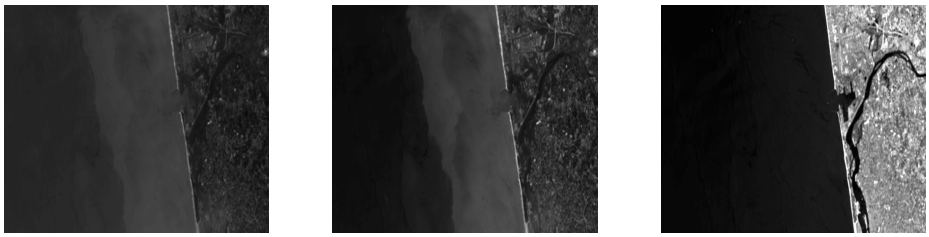

(a) B band (b) G band (c) NIR band

Figure 4.8 Low pass filter of band B, G and NIR

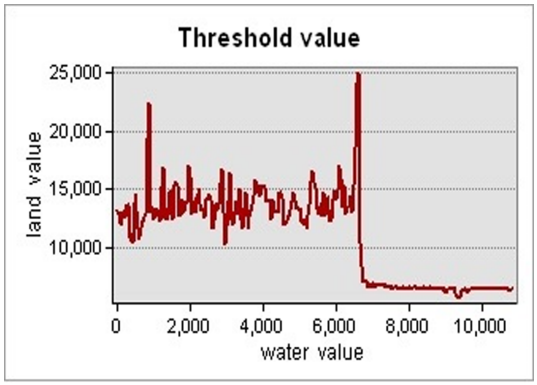

Figure 4.9 Threshold value to separate the land from water

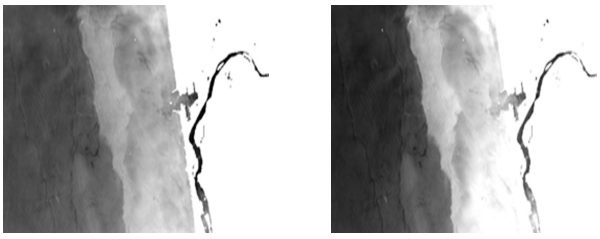

(a) B band (b) G band

Figure 4.10 Removal of land from water for B and G bands

Secondly, linear regression is established for all the selected area of each visible band against the NIR band as shown in Figs. 4.12(a) for B band and 4.12(b) for G band, where x-axis represents the NIR band brightness and y-axis represents the visible band. To remove the sun glint and cloud, the following parameters such as R_i, b_i, R_{NIR} and Min_{NIR} are needed. R_i is the pixel value in the corresponding B and G bands, the regression slope b_i is calculated for the band B and G using the following equation.

(a) B band (b) G band

Figure 4.11 Extraction of polygon for band B and G

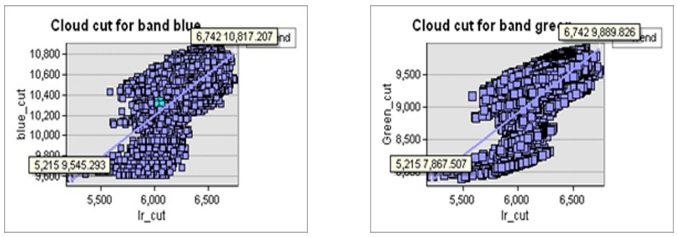

(a) B band (b) G band

Figure 4.12 Linear regression is established to determine the Min_{NIR}

$$\text{Slope} = \frac{y_2 - y_1}{x_2 - x_1} \tag{4.1}$$

Where, the value of x_1, x_2, y_1, y_2 and the value of Min_{NIR} (pixel brightness of NIR) are obtained from Fig. 4.12(a) for band B and 4.12(b) for band G. R_{NIR} is the pixel value of NIR band. Consequently, the removal of sun glint of band B and G are shown in Figs. 4.13(a) and 4.13(b).

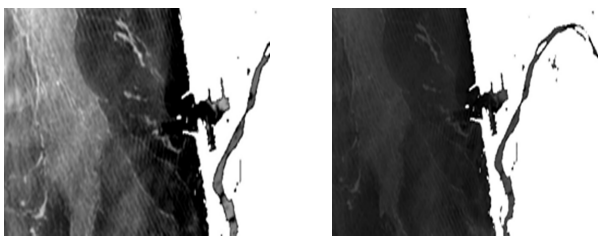

(a) B band (b) G band

Figure 4.13 Removal of sun glint for band B and G

The ratio transform algorithm is adopted on the pre-processed B and G bands, the important requirement for estimating the bathymetry of near-shore ocean using

the ratio transform algorithm is reference depth value (hydrographic chart). The hydrographic chart is prepared by using the in-situ data; collected using multi beam echo sounders and it is corrected to mean lower low water (MLLW). The outcome of $\ln(L_{obs}(Band_{blue}))/\ln(L_{obs}(Band_{green}))$ (i.e. named as bathy image) is shown in Fig. 4.14(a). The reference depth value (hydrographic chart) is overlaid on the bathy image and is shown in the Fig. 4.14(b). The pixel value of the bathy image is obtained with the reference of hydrographic chart value and so there is no need to measure the tidal height during the image acquisition(Pe'eri et al., 2014).

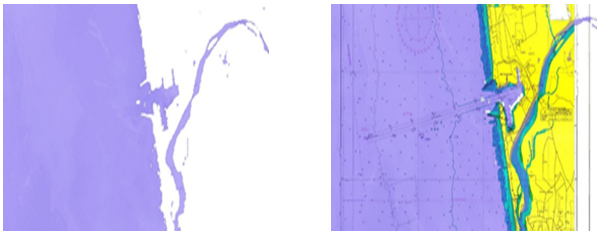

(a) Bathy image

(b) Hydrogarphic chart overlaid on bathy image

Figure 4.14 Represents the bathy image and hydrographic chart overlaid on bathy image

To study the effectiveness of improving the spatial resolution of Landsat-8 imagery. The original B and G bands with the spatial resolution of 30 m is fused separately with the Pan band of 15 m spatial resolution. Improved spatial resolution of band B and G obtained using the Fuze Go pan-sharpening method are shown in the Figs. 4.15(a) and (b). The same procedure for estimating the bathymetry of near-shore is adopted on the improved spatial resolution of B and G bands, and the results obtained before and after improving the spatial resolution are compared.

The depth points in the hydrographic chart and the corresponding pixel values from the bathy image are obtained and the scatter plot is plotted which is shown in Figs. 4.16(a) and (b) for before and after improving the spatial resolution in which, x-axis represents the hydrographic chart depth and y-axis represents the corresponding pixel value. To estimate the bathymetry of near-shore ocean using ratio transform algorithm, certain parameters are required such as *Lobs*, m_1 and m_0 where, *Lobs* are observed

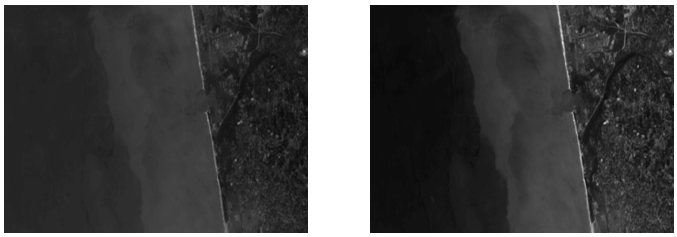

(a) B band (b) G band

Figure 4.15 Improved spatial resolution of blue and green band

radiance of bands, obtained from the ratio of band blue and green which is shown in Fig. 4.14(a) and m_1 and m_0 are obtained empirically by correlating the corresponding pixel value to the hydrographic chart value [Figs 4.16(a) and (b)] are shown in the Tables 4.9 and 4.10 .

Table 4.9 m_1 and m_0 values before improving the spatial resolution of Landsat-8 imagery

Range of Depth (m)	m_1	m_0
0-5	155.16	172.09
5-16	148.42	158.7
16 -25	143.9	147.36

Table 4.10 m_1 and m_0 values after improving the spatial resolution of Landsat-8 imagery

Range of Depth (m)	m_1	m_0
0-10	316.9	353.9
10-16	123.47	130.05
16 -25	81.09	86.668

The effectiveness of improving the spatial resolution of Landsat-8 imagery for determining the bathymetry of near-shore ocean is examined by comparing the results of both (i.e. before improving the spatial resolution 30 m and after improving the spatial resolution to 15 m by Fuze Go method). To validate the ratio transform algorithm, the

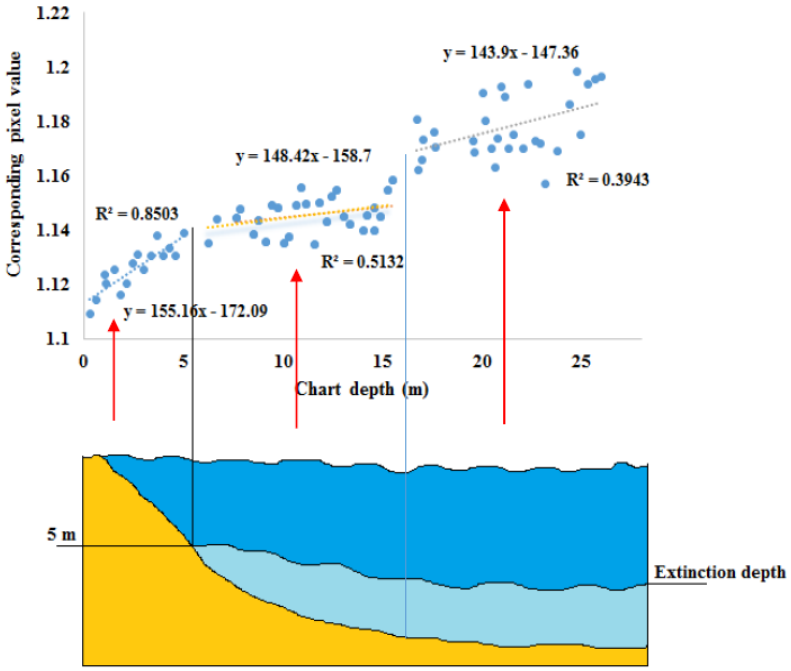

(a) Before improving

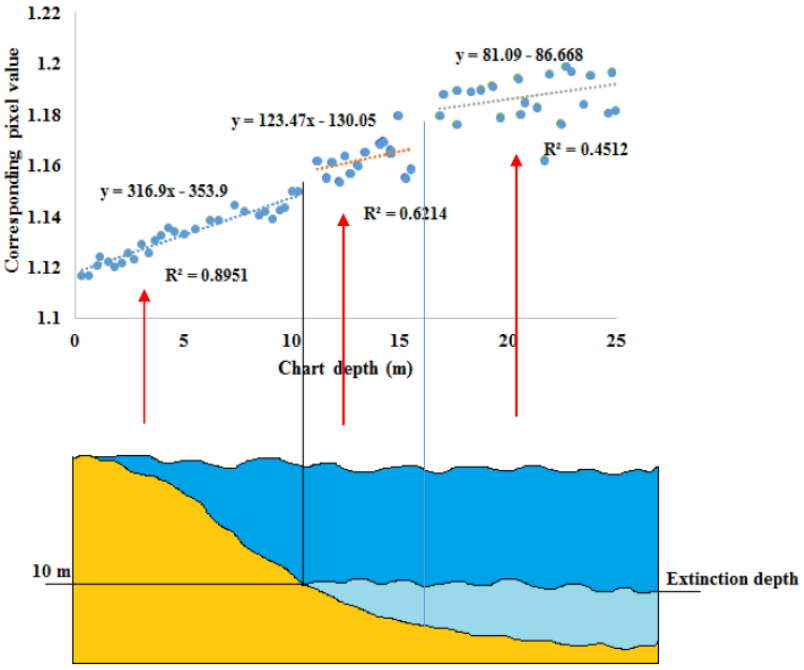

(b) After improving

Figure 4.16 Extinction of depth before and after improving the spatial resolution

statistical index such as RMSE and MAE is computed between the algorithm results and hydrographic chart depth.

The Fig. 4.16(a) represents the result of estimating the bathymetry of near-shore ocean before improving the spatial resolution of satellite image (i.e. 30 m), where the top portion of the image shows the scatter plot of the corresponding pixel value against the hydrographic chart depth, which indicates good correlation value of $R^2 = 0.8503$ for depth up to 5 m. It is also seen that the value of $R^2 = 0.5132$ for the depth from 5 to 16 m indicates that the pixel value moderately match the hydrographic chart depth and the value of $R^2 = 0.3943$ for the depth from 16 to 25 m indicates that the pixel value and hydrographic chart depth do not match.

The bottom portion of the image explains the pixel value and their relation to the depth of extinction. Areas deeper than the extinction depth (i.e. 5 m) do not have a good correlation between the pixel value and the reference hydrographic chart depth. Therefore, the ratio transform algorithm can retrieve the depth up to 5 m for the 30 m spatial resolution of Landsat-8 imagery.

The Fig. 4.16(b) represents the result of estimating the bathymetry of near-shore ocean (i.e. after improving the spatial resolution of satellite image to 15 m), where the top portion of the image shows the scatter plot of the corresponding pixel value against the hydrographic chart depth which indicates the good correlation value of $R^2 = 0.8951$ for the depth up to 10 m. It is also seen that the value of $R^2 = 0.6214$ for the depth from 10 to 16 m indicates that the pixel value moderately match the hydrographic chart depth and the value of $R^2 = 0.4512$ for the depth from 16 to 25 m indicates that the pixel value and hydrographic chart depth matches unlikely.

The bottom portion of the image explains that the areas deeper than the extinction depth 10 m do not have a good correlation between the pixel value and the reference hydrographic chart depth. Therefore, it is evident that improving the spatial resolution of satellite image helps to determine the higher depth precisely.

The required parameters such as *Lobs* (obtained from the ratio of band blue and green), m_1 and m_0 (obtained empirically by correlating the corresponding pixel value to the hydrographic chart value) are provided as input to the ratio transform algorithm and obtained depth z. Further, the parameter m_1 is fine tuned for producing better matches between the algorithm results and the reference hydrographic chart value. To validate

the ratio transform algorithm, the statistical index such as RMSE and MAE is computed between the algorithm results and hydrographic chart depth is shown in the Tables 4.11 and 4.12.

Table 4.11 RMSE and MAE values before improving the spatial resolution of Landsat-8 imagery

Range of Depth (m)	RMSE (m)	MAE (m)
0-5	0.94	0.89
5-16	2.51	2.47
16 -25	5.63	5.59

Table 4.12 RMSE and MAE values after improving the spatial resolution of Landsat-8 imagery

Range of Depth (m)	RMSE (m)	MAE (m)
0-10	0.86	0.79
10-16	2.39	2.25
16 -25	5.21	5.09

Table 4.11 indicates that the range of depth between 0-5 m has higher accuracy (RMSE = 0.94; MAE=0.89). From Table 4.12 it is observed that the highest accuracy of (RMSE=0.86; MAE=0.79) is achieved for the range of depth between 0-10 m. Therefore, the ratio transform algorithm can better estimate the depth up to 10 m for the improved spatial resolution of Landsat-8 imagery.

Figs. 4.17(a) and (b) represents the estimation of bathymetry before and after improving the spatial resolution of satellite image along the coast of Mangaluru, Karnataka. The Landsat-8 image with the spatial resolution of 30 m provided better estimation of depth up to 5 m which is indicated in light blue and shown in Fig. 4.17(a) and the depth from 5 to 16 m is shown in blue and the depth from 16 to 25 m are shown in dark blue in which the algorithm results and hydrographic chart depth do not match. Therefore, the Landsat-8 image with spatial resolution of 30 m better estimates the depth up to 5 m.

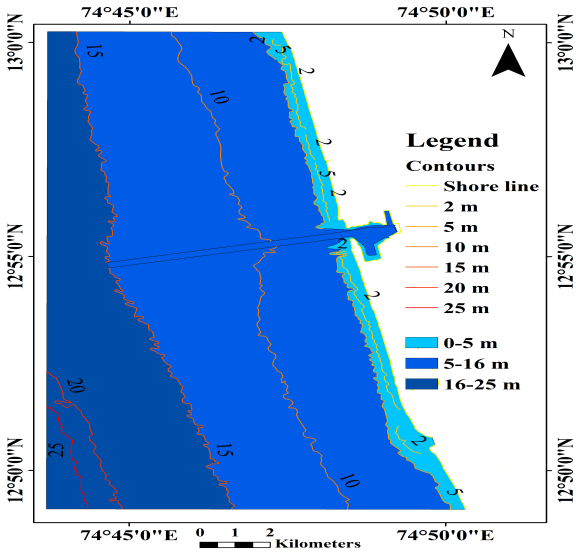

(a) Before improving

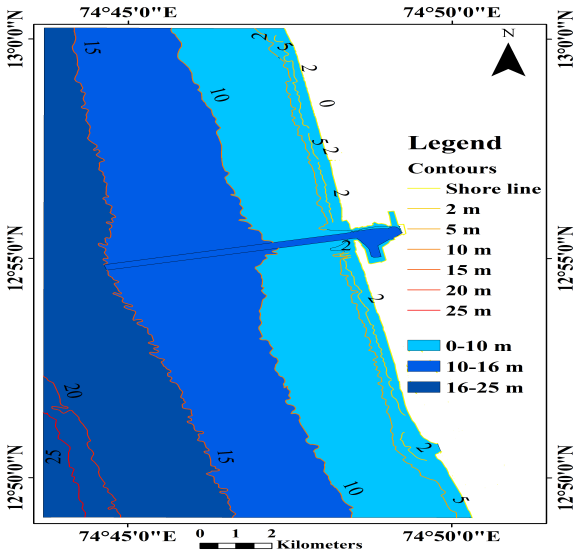

(b) After improving

Figure 4.17 Estimation of depth before and after improving the spatial resolution

The Landsat-8 image with the spatial resolution of 15 m can better estimate the depth up to 10 m (which is coloured in light blue) is shown in Fig. 4.17(b) and the depth from 10 to 16 m is shown in blue and the depth from 16 to 25 m is shown in dark blue indicates that the algorithm results and hydrographic chart depth do not match. Therefore, the Landsat-8 image with improved spatial resolution of 15 m better estimates the depth up to 10 m.

Chapter 5

CONCLUSIONS

5.1 General

The study focused on improving the spatial resolution of multispectral imagery of Landsat-8 and Quickbird-2 using nine pan-sharpening techniques. Further, all of the pan-sharpened image generated by the pan-sharpening techniques were evaluated using qualitative and quantitative approaches. In addition, the effectiveness of improving the spatial resolution of multispectral imagery of Landsat-8 and Quickbird-2 was studied by employing the best pan-sharpened image for the extraction of buildings and for estimating the bathymetry of near-shore ocean. The automatic and manual approaches were adopted to extract the buildings from the original MS and pan-sharpened imagery of Quickbird-2. Furthermore, the procedure based on the ratio-transform algorithm for estimating the near-shore bathymetry was adopted on original B, G and pan-sharpened imageries of Landsat-8.

The key conclusions framed after analysing the results obtained and subsequent discussion, have been presented this chapter with brief summary for convenience. Also, limitations of the study and future scope for further studies are enumerated.

5.1.1 Pan-sharpening the multispectral imagery of Quickbird-2 and Landsat-8 and quality evaluation using qualitative and quantitative analysis

In this study, nine different pan-sharpening methods like PCA, M-IHS, Multiplicative BT, W-PCA, HCS, HPF, GS and Fuze Go were applied to fuse Pan and MS imageries of Landsat-8 as well as Quickbird-2. The pan-sharpened images obtained for each

of the pan-sharpening methods were evaluated and compared using quantitative and qualitative (or) visual approaches. In quantitative analysis the spectral indices like CC, SSIM, RMSE, SNR, PSNR and Q were used to assess the spectral quality of pan-sharpened image. The spatial indices like SCC, Gradient and image entropy were used to assess the spatial quality of pan-sharpened image. Further, QNR indices was also performed to evaluate both spectral and spatial quality of pan-sharpened image. The inputs from the qualitative and quantitative analysis were considered for the selection of best pan-sharpened image. Following conclusions are drawn from the present study:

- The qualitative assessment of the pan-sharpened images revealed that all of the pan-sharpening methods increased the spatial detail in the fused image. However, the multiplicative method generated an unsatisfactory fused image with high spatial and spectral distortion. The BT and HCS methods best preserved the spectral information but retained fewer spatial details.

- The PCA method improved the spatial details but generated colour distortion. Although the M-IHS and W-PCA methods improved the spatial details and preserved the spectral information, the results were not as good as those obtained by Fuze Go, HPF, and GS. Visual assessment of the pan-sharpened image revealed that the Fuze Go method generated the pan-sharpened image with the highest spatial and spectral quality followed by HPF and GS.

- The results from seven of the ten quantitative indices revealed that the Fuze Go method ranked first followed by HPF and GS methods. The assessment results of qualitative and quantitative analyses also showed that the Fuze Go method performed better than the other pan-sharpening methods. It is also noticeable that the multiplicative method ranked last by both qualitative and quantitative analyses. Hence, a general agreement was observed among the results of the two analyses.

- The Fuze Go method was able to produce the image with the highest spatial details and rich spectral information, can be used for identifying and differentiating

small features spatially and spectrally. This method can be used for remote sensing applications like feature extraction, urban planning, classification, etc.

5.1.2 Extraction of buildings

In this study, automatic and manual approaches were adopted to extract the buildings from the original MS and Fuze Go pan-sharpened imagery of Quickbird-2. In the automatic approach, firstly the vegetation portion was removed, secondly adaptive k means clustering algorithm was performed to classify the pixels into a number of classes which then was followed using morphological operators to extract the buildings. The performance of automatic approach for the both imageries were compared using quantitative and qualitative analysis. The manual method was also adopted to study the effectiveness of improved spatial resolution of the original MS imagery for the extraction of buildings and are compared qualitatively. Following conclusions were derived from this study:

- From the results of automatic approach, it is visualized that the major buildings are detected correctly for the original MS and pan-sharpened image. However, the loss of information is evident in both the images. The results of manual method indicate that the extraction of buildings is achieved with minimum loss of information in comparison with the automatic method.

- The results from both the automatic and manual methods of pan-sharpened image indicate that the spatial and spectral information of buildings are clearly identifiable. Therefore, improving the spatial resolution of the original MS image increases the spatial and spectral information of buildings.

- In the case of any input image (i.e. if the interested features are identified to be different from each other in terms of shape, size and color), manual method is recommended, in order to reduce loss of information. However, the effectiveness of the method depends on the user experience and it is a time consuming process.

- It is to be noted that the performance of automatic algorithm is effective when all buildings are in rectangular shape. In our case, the building shapes are different

from one another and nevertheless, the performance of automatic approach for the extraction of buildings with different shape, size and color is reasonable.

5.1.3 Estimation of Bathymetry

The procedure based on the ratio transform algorithm was adopted to determine the bathymetry of near-shore ocean along the coast of Mangaluru, India using Landsat-8 imagery. The effectiveness of improving the spatial resolution of B and G bands was studied by employing the procedure on the original and pan-sharpened imageries of Landsat-8, and the results of both the imageries were compared using RMSE and MAE indices. Following conclusions are derived from this study:

- The procedure can be best used as an exploration tool to infer the bathymetry of coastal region before a high resolution hydrographic survey is operated using an expensive instrument like multi-beam echo sounder etc.

- The results of satellite image show a good correlation of $R^2 = 0.8503$ with the hydrographic chart data for the depth up to 5 m for the 30 m spatial resolution of Landsat-8 imagery.

- The results of satellite image after improving the spatial resolution to 15 m, show a good correlation of $R^2 = 0.8951$ with the hydrographic chart data for depths up to 10 m. Therefore, improving the spatial resolution helps to infer higher depths in the coastal region.

- The results of RMSE and MAE between the ratio transform algorithm and hydrographic chart indicates that the algorithm better estimates the depth up to 10 m for the improved spatial resolution of Landsat-8 imagery.

- The procedure used for deriving the satellite bathymetry can be used by marine surveyors and hydrographic officers. By using the results of this procedure, marine surveyors can assess the current amount of change in depth, and if a weaker R^2 value is observed, it necessitates the updation of high resolution hydrographic chart to the existing one.

- To derive the bathymetry using the satellite imagery, environmental conditions such as water clarity, cloud cover, a sun glint is needed to be considered that could deteriorate the accuracy of estimated depth.

- It is also to be noted that the selection of reference hydrographic chart is important; due to the age of the hydrographic survey or the old technique and equipment used to conduct the survey.

- Finally, regardless of improvement in the satellite derived bathymetry, the procedure evolved can be used as an exploration tool for operating the hydrographic survey and this is not an alternative for acoustic hydrographic survey.

5.2 Limitation of study

- The pan-sharpening techniques are not processed for cross sensor satellite imagery.

- The close acquisition date of satellite image and sounding data was available only for NMPT regions which restricted the validation of procedure for estimating the bathymetry of different regions.

5.3 Future scope of study

- Pan-sharpening the cross sensor imagery.

- Evaluation of pan-sharpening techniques using classification methods.

5.4 Acknowledgements

- S.Pe'eri, B.Madore and L.Alexander (Center for Coastal and Ocean Mapping, USA), C.Parrish and A.Armstrong (National Oceanic and Atmospheric Administration, USA), C.Azuike (Nigerian Navy Hydrogarphic office Lagos), Nigerian and Eunice N.Tetteh (Ghana National Oceanographic data center, Ghana).

- Dr. Richard P. Stumpf, Oceanographer, NOAA (National Center for Coastal Ocean Science) and Dr. Shachak Pe'eri, Research Associate Professor, Center

for Coastal and Ocean Mapping, University of New Hampshire for providing the necessary support for research execution.

- The support from the authorities of New Mangaluru Port Trust (NMPT), Mangaluru, Karnataka, India for providing the necessary data required for research and also lending a hand to understand the working of echo sounder instrument.

Bibliography

Alimuddin, I., Sumantyo, J. T. S., and Kuze, H. (2012). "Assessment of pan-sharpening methods applied to image fusion of remotely sensed multi-band data". *International Journal of Applied Earth Observation and Geoinformation*, 18, 165–175.

Alparone, L., Aiazzi, B., Baronti, S., Garzelli, A., Nencini, F., and Selva, M. (2008). "Multispectral and panchromatic data fusion assessment without reference". *Photogrammetric Engineering & Remote Sensing*, 74(2), 193–200.

Alparone, L., Baronti, S., Garzelli, A., and Nencini, F. (2004). "A global quality measurement of pan-sharpened multispectral imagery". *IEEE Geoscience and Remote Sensing Letters*, 1(4), 313–317.

Alparone, L., Wald, L., Chanussot, J., Member, S., Thomas, C., Gamba, P., and Bruce, L. M. (2007). "Comparison of pansharpening algorithms : Outcome of the 2006 grss data-fusion contest". *IEEE Transactions on Geoscience and Remote Sensing*, 45(10), 3012–3021.

Amolins, K., Zhang, Y., and Dare, P. (2007). "Wavelet based image fusion techniques-an introduction, review and comparison". *ISPRS Journal of Photogrammetry and Remote Sensing*, 62(4), 249–263.

Amro, I., Mateos, J., Vega, M., Molina, R., and Katsaggelos, A. K. (2011). "A survey of classical methods and new trends in pansharpening of multispectral images". *EURASIP Journal on Advances in Signal Processing*, 2011(1), 1–22.

Ashraf, S., Brabyn, L., and Hicks, B. J. (2012). "Image data fusion for the remote sensing of freshwater environments". *Applied Geography*, 32(2), 619–628.

Attarzadeh, R. and Momeni, M. (2012). "Object-based building extraction from high resolution satellite imagery". *International Archives of the Photogrammetry*, 29-B4(September), 57–60.

Brando, V. E., Anstee, J. M., Wettle, M., Dekker, A. G., Phinn, S. R., and Roelfsema, C. (2009). "A physics based retrieval and quality assessment of bathymetry from suboptimal hyperspectral data". *Remote Sensing of Environment*, 113(4), 755–770.

Burt, P. and Adelson, E. (1983). "The laplacian pyramid as a compact image code". *IEEE Transactions on Communications*, 31(4), 532–540.

Carper, W. J., Lillesand, T., and Kiefer, R. (1994). "The use of intensity hue saturation transform for merging spot panchromatic and multispectral image data". *Photogrammetric Engineering and Remote Sensing*, 60(11), 1369–1374.

Carron, M. J., Vogt, P. R., and Jung, W. (2001). "A proposed international long-term project to systematically map the world's ocean floors from beach to trench: Gomap (global ocean mapping program)". *Inter. Hydr. Rev.*, 2(3), 49–50.

Chai, Y., Li, H., and Zhang, X. (2012). "Multifocus image fusion based on fetaures contrast of multiscale products in nonsubsampled contourlet transform". *Optik*, 123(7), 1–4.

Chaudhuri, D., Kushwaha, N. K., Samal, A., and Agarwal, R. C. (2016). "Automatic building detection from high-resolution satellite images based on morphology and internal gray variance". *IEEE Journal of Selected Topics in Applied Earth Observations and Remote Sensing*, 9(5), 1767–1779.

Chavez, P., Sides, S. C., and Anderson, J. A. (1991). "Comparison of three different methods to merge multi resolution and multispectral data:landsat tm and spot panchromatic". *Photogrammetric Engineering & Remote Sensing*, 57(03), 295–303.

Chavez, P. S. T. and Kwarteng, A. Y. (1989). "Extracting spectral constrast in landsat thematic mapper image data using selective principal component analysis". *Photogrammetric Engineering and Remote Sensing*, 55(3), 339–348.

Chen, C. W., Luo, J., and Parker, K. J. (1998). "Image segmentation via adaptive k-mean clustering and knowledge-based morphological operations with biomedical applications". *IEEE Transactions on Image Processing*, 7(12), 1673–1683.

Cheng, J., Liu, H., Liu, T., Wang, F., and Li, H. (2015). "Remote sensing image fusion via wavelet transform and sparse representation". *Isprs Journal of Photogrammetry and Remote Sensing*, 104, 158–173.

Choi, M. (2006). "A new intensity-hue-saturation fusion approach to image fusion with a tradeoff parameter". *IEEE Transactions on Geoscience and Remote Sensing*, 44(6), 1672–1682.

Crippen, R. E. (1989). "A simple spatial filtering routine for the cosmetic removal of scan-line noise from landsat tm p-tape imagery". *Photogrammetric Engineering and Remote Sensing*, 55(3), 327–331.

Dekker, A. G., Phinn, S. R., Anstee, J., Bissett, P., Brando, V. E., Casey, B., Fearns, P., Hedley, J., Klonowski, W., and Lee, Z. P. (2011). "Intercomparison of shallow water bathymetry, hydro-optics, and benthos mapping techniques in australian and caribbean coastal environments". *Limnology and Oceanography: Methods*, 9, 396–425.

Doxani, G., Papadopoulou, M., Lafazani, P., Pikridas, C., and Tsakiri-Strati, M. (2012). "Shallow-water bathymetry over variable bottom types using multispectral worldview-2 image". *ESA 2nd Space for Hydrology Workshop*, 14853(1), 159–164.

Du, P., Liu, S., Xia, J., and Zhao, Y. (2013). "Information fusion techniques for change detection from multi-temporal remote sensing images". *Information Fusion*, 14(1), 19–27.

Du, Q., Younan, N. H., King, R., and Shah, V. P. (2007). "On the performance evaluation of pan-sharpening techniques". *IEEE Geoscience and Remote Sensing Letters*, 4(4), 518–522.

Ehlers, M. E. D.-M., Kolouch, D., Lohman, P., and Dennert-Möller, E. (1984). Non-recursive Filter Techniques in Digital Processing of Remote Sensing Imagery. In *International society for photogrammetry and Remote sensing*, 163–175.

Eugenio, F., Marcello, J., and Martin, J. (2015). "High-resolution maps of bathymetry and benthic habitats in shallow-water environments using multispectral remote sensing imagery". *IEEE Transactions on Geoscience and Remote Sensing*, 53(7), 3539–3549.

Fonseca, L., Namikawa, L., and Castejon, E. (2011). "Image fusion for remote sensing applications". *InTech*, 153–158.

Fonseca, L. M. G., Costa, M. H. M., Korting, T. S., Castejon, E., and Silva, F. C. (2008). "Multitemporal image registration based on multiresolution decomposition". *Revista Brasileira de Cartografia*, 271–286.

Fowler, J. E. and Member, S. (2005). "The redundant discrete wavelet transform and additive noise". *IEEE signal processing letters*, 12(9), 629–632.

Gangkofner, U. G., Pradhan, P. S., and Holcomb, D. W. (2008). "Optimizing the high-pass filter addition technique for image fusion". *Photogrammetric Engineering & Remote Sensing*, 74(9), 1107–1118.

Gao, J. (2009). "Bathymetric mapping by means of remote sensing: methods, accuracy and limitations". *Progress in Physical Geography*, 33(1), 103–116.

Ghaffarian, S. and Ghaffarian, S. (2014). "Automatic building detection based on purposive fastica (pfica) algorithm using monocular high resolution google earth images". *ISPRS Journal of Photogrammetry and Remote Sensing*, 97, 152–159.

Ghosh, A. and Joshi, P. (2013). "Assessment of pan-sharpened very high-resolution worldview-2 images". *International Journal of Remote Sensing*, 34(23), 8336–8359.

Giardino, C., Candiani, G., Bresciani, M., Lee, Z., Gagliano, S., and Pepe, M. (2012). "Bomber: A tool for estimating water quality and bottom properties from remote sensing images". *Comput. Geosci.*, 45, 313–318.

Gillespie, A. R., Kahle, A. B., and Walker, R. E. (1987). "Color enhancement of highly correlated images. ii. channel ratio and chromaticity transformation techniques". *Remote Sensing of Environment*, 22(3), 343–365.

Gonzalez-Audicana, M., Otazu, X., Fors, O., and Seco, A. (2005). "Comparison between mallat's and the atrous discrete wavelet transform based algorithms for the fusion of multispectral and panchromatic images". *International Journal of Remote Sensing*, 26(3), 595–614.

Hallada, W. and Cox, S. (1983). "Image sharpening for mixed spatial and spectral resolution satellite systems". *International Sysmposium on Remote Sensing of the Environment.*, 17, 9–13.

Hedley, J. D., Harborne, A. R., and Mumby, P. J. (2005). "Technical note: Simple and robust removal of sun glint for mapping shallow water benthos". *International Journal of Remote Sensing*, 26(10), 2107–2112.

Hochberg, E. J., Andréfouët, S., and Tyler, M. R. (2003). "Sea surface correction of high spatial resolution ikonos images to improve bottom mapping in near-shore environments". *IEEE Transactions on Geoscience and Remote Sensing*, 41(7 PART II), 1724–1729.

Jiang, Y. and Wang, M. (2014). "Image fusion with morphological component analysis". *Information Fusion*, 18(1), 107–118.

King, R. and Wang, J. (2001). "A wavelet based algorithm for pan sharpening landsat 7 imagery". *proceedings of the international of geoscience and remote sensing symposium (IGARSS 2001).*, 2(C), 849–851.

Kingsbury, N. (1999). "Image processing with complex wavelets". *Philosophical Transactions of the Royal Society A: Mathematical, Physical and Engineering Sciences*, 357(1760), 2543–2560.

Kumar, H. and Singh (2010). "Quality assessment of fused image of modis and palsar". *Progress In Electromagnetics Research*, 24(June), 191–221.

Laben, C. and Brower, B. (2000). "Process for enhancing the spatial resolution of multispectral imagery using pan-sharpening". *US Patent 6,011,875*, 1–8.

Leung, Y., Liu, J., and Zhang, J. (2014). "An improved adaptive intensity-hue- saturation method for the fusion of remote sensing images". *IEEE Geoscience and Remote Sensing Letters*, 11(5), 985–989.

Liasis, G. and Stavrou, S. (2016). "Building extraction in satellite images using active contours and colour features". *International Journal of Remote Sensing*, 37(5), 1127–1153.

Lin, C. and Nevatia, R. (1998). "Building detection and description from a single intensity image". *Computer Vision and Image Understanding*, 72(2), 101–121.

Lyzenga, D. R. (1981). "Remote sensing of bottom reflectance and water attenuation parameters in shallow water using aircraft and landsat data". *International Journal of Remote Sensing*, 2(1), 71–82.

Lyzenga, D. R., Malinas, N. P., and Tanis, F. J. (2006). "Multispectral bathymetry using a simple physically based algorithm". *IEEE Transactions on Geoscience and Remote Sensing*, 44(8), 2251–2259.

Mayer, H. (1999). "Automatic object extraction from aerial imagery–a survey focusing on buildings". *Computer Vision and Image Understanding*, 74(2), 138–149.

Mishra, D. R., Narumalani, S., Rundquist, D., Lawson, M. P., and Perk, R. (2007). "Enhancing the detection and classification of coral reef and associated benthic habitats: A hyperspectral remote sensing approach". *Journal of Geophysical Research*, 112, C08014.

Mobley, C. D., Sundman, L. K., Davis, C. O., Bowles, J. H., Downes, T. V., Leathers, R. A., Montes, M. J., Bissett, W. P., Kohler, D. D. R., Reid, R. P., Louchard, E. M., and Gleason, A. (2005). "Interpretation of hyperspectral remote-sensing imagery by spectrum matching and look-up tables". *Appl. Opt.*, 44(17), 3576–3592.

Naidu, V. P. S. (2010). "Discrete cosine transform-based image fusion". *Defence Science Journal*, 60(1), 48–54.

Nejati, M., Samavi, S., and Shirani, S. (2015). "Multi-focus image fusion using dictionary-based sparse representation". *Information Fusion*, 25, 72–84.

Nikolakopoulos, K. G. (2008). "Comparison of nine fusion techniques for very high resolution data". *Photogrammetric Engineering & Remote Sensing*, 74(5), 647–659.

Padwick, C., Deskevich, M., Pacifici, F., and Smallwood, S. (2010). "Worldview-2 pan-sharpening". *Asprs 2010*, 48(1), 26–30.

Pappas, T. N. (1992). "An adaptive clustering algorithm for image segmentation". *IEEE Transactions on Signal Processing*, 10(4), 901–914.

Pattanaik, A., Sahu, K., and Bhutiyani, M. R. (2015). "Estimation of shallow water bathymetry using irs-multispectral imagery of odisha coast, india". *Aquatic Procedia*, 4(0), 173–181.

Pe'eri, S., Parrish, C., Azuike, C., Alexander, L., and Armstrong, A. (2014). "Satellite remote sensing as a reconnaissance tool for assessing nautical chart adequacy and completeness". *Marine Geodesy*, 37(3), 293–314.

Petrovic, V. S. and Xydeas, C. S. (2004). "Gradient-based multiresolution image fusion". *IEEE transactions on image processing : a publication of the IEEE Signal Processing Society*, 13(2), 228–37.

Philpot, W. D. (1989). "Bathymetric mapping with passive multispectral imagery". *Appl. Opt.*, 28(8), 1569–1578.

Ranchin, T. and Wald, L. (2000). "Fusion of high spatial and spectral resolution images: The arsis concept and its implementation". *Photogrammetric Engineering and Remote Sensing*, 66(1), 49–61.

Segl, K. and Kaufmann, H. (2001). "Detection of small objects from high-resolution panchromaticsatellite imagery based on supervised image segmentation". *IEEE*

Transactions on Geoscience and Remote Sensing and Remote Sensing, 39(9), 2080–2083.

Shahdoosti, H. R. and Ghassemian, H. (2015). "Fusion of ms and pan images preserving spectral quality". *IEEE Geoscience and Remote Sensing Letters*, 12(3), 611–615.

Sheng, M., Tao, Z., Yang, X., Yu, Y., Zhou, X., and Li, Z. (2014). "Bathymetry retrieval from hyperspectral remote sensing data in optical-shallow water". *IEEE Transactions on Geoscience and Remote Sensing*, 52(2), 1205–1212.

Shorter, N. and Kasparis, T. (2009). "Automatic vegetation identification and building detection from a single nadir aerial image". *Remote Sensing*, 1(4), 731–757.

Siddiqui, Y. (2003). "The modified ihs method for fusing satellite imagery". *In Proceedings of the ASPRS 2003 annual conference*, 153–158.

Song, H., Huang, B., Liu, Q., and Zhang, K. (2015). "Improving the spatial resolution of landsat tm/etm+ through fusion with spot5 images via learning-based super-resolution". *IEEE T Geosci. Remote*, 53(3), 1195–1204.

Spitzer, D. and Dirks, R. W. J. (1986). "Classification of bottom composition and bathymetry of shallow waters by passive remote sensing". *Proc. of the 7th ISPRS Commission VII Symp., Remote Sensing for Resources Development and Environmental Management*, 2(2), 775–777.

Stumpf, R. P., Holderied, K., and Sinclair, M. (2003). "Determination of water depth with high-resolution satellite imagery over variable bottom types". *Limonology And Oceanography*, 48(48/1, part 2), 547–556.

Su, H., Liu, H., and Heyman, W. D. (2008). "Automated derivation of bathymetric information from multi-spectral satellite imagery using a non-linear inversion model". *Marine Geodesy*, 31(May), 281–298.

Su, H., Liu, H., Wang, L., Filippi, A. M., Heyman, W. D., and Beck, R. A. (2014). "Geographically adaptive inversion model for improving bathymetric retrieval from

satellite multispectral imagery". *IEEE Transactions on Geoscience and Remote Sensing*, 52(1), 465–476.

Vahtmäe, E. and Kutser, T. (2016). "Airborne mapping of shallow water bathymetry in the optically complex waters of the baltic sea". *Journal of Applied Remote Sensing*, 10(2), 025012.

Vandermeer, F. (2006). "The effectiveness of spectral similarity measures for the analysis of hyperspectral imagery". *International Journal of Applied Earth Observation and Geoinformation*, 8(1), 3–17.

Wald, L. (2000). "Quality of high resolution synthesised images: is there a simple criterion". 99–103.

Wang, M., Yuan, S., and Pan, J. (2013). "Building detection in high resolution satellite urban image using segmentation, corner detection combined with adaptive windowed hough transform ". In *Geoscience and Remote Sensing Symposium (IGARSS), 2013 IEEE International*, 508–511.

Wang, W. and Chang, F. (2011). "A multi-focus image fusion method based on laplacian pyramid". *Journal of Computers*, 6(12), 2559–2566.

Wang, Z. and Bovik, A. C. (2002). "A universal image quality index". *IEEE singal Processing Letter*, XX(Y), 2–5.

Wang, Z., Bovik, A. C., Sheikh, H. R., Member, S., Simoncelli, E. P., and Member, S. (2004). "Image quality assessment : From error visibility to structural similarity". *IEEE Transactions on Image Processing*, 13(4), 1–14.

Winterbottom, S. J. and Gilvear, D. J. (1997). "Quantification of channel bed morphology in gravel-bed rivers using airborne multispectral imagery and aerial photography". *Regulated Rivers: Research and Management*, 13(6), 489–499.

Wu, B., Fu, Q., Sun, L., and Wang, X. (2015). "Enhanced hyperspherical color space fusion technique preserving spectral and spatial content". *Journal of Applied Remote Sensing*, 9, 097291–18.

Xu, Q., Zhang, Y., Li, B., and Ding, L. (2015). "Pansharpening using regression of classified ms and pan images to reduce color distortion". *IEEE Geoscience and Remote Sensing Letters*, 12(3), 1–5.

Yang, B., Jing, Z., and Zhao, H. (2010). "Review of pixel-level image fusion". *Journal of Shanghai Jiaotong University (Science)*, 15(1), 6–12.

Yuhendra, Alimuddin, I., Sumantyo, J. T. S., and Kuze, H. (2012). "Assessment of pan-sharpening methods applied to image fusion of remotely sensed multi-band data ". *International Journal of Applied Earth Observation and Geoinformation*, 18, 165 – 175.

Yusuf, Y., Sri Sumantyo, J. T., and Kuze, H. (2012). "Spectral information analysis of image fusion data for remote sensing applications". *Geocarto International*, 28(4), 291–310.

Zhang, J. (2010). "Multi-source remote sensing data fusion: status and trends". *International Journal of Image and Data Fusion*, 1(1), 5–24.

Zhang, Y. (2004). "System and method for image fusion". *US Patent 7,340,099*, 1–14.

Zhang, Y. and Mishra, R. K. (2013). "From unb pansharp to fuze go-the success behind the pan-sharpening algorithm". *International Journal of Image and Data Fusion*, 5(1), 39–53.

Zheng, P., Deng, Z., and Ye, X. (2014). "Retrieval study of lake water depth by using multi-spectral remote sensing in bangong co lake". *Sciences in Cold and Arid Regions*, 6(3), 266–272.

Zoran, L. F. (2009). "Quality evaluation of multiresolution remote sensing image fusion". *U.P.B. Sci. Bull., Series C*, 71(3), 38–52.

5.5 List of Publications /Communications based on Thesis:

5.5.1 Journal papers

- Jagalingam P and Arkal Vittal Hegde (2016). "Evaluation of Pan-sharpening methods for spatial and spectral quality". Applied Geomatics, Springer, online, DOI: 10.1007/s12518-016-0179-2.

- Jagalingam P and Arkal Vittal Hegde (2017). "Estimation of bathymetry along the coast of Mangaluru using Landsat-8 Imagery". International journal of ocean and climate systems, Sage Publication, online, DOI: 10.1177/1759313116679672.

- Jagalingam P and Arkal Vittal Hegde (2017). "Comparison of various Pan-sharpening methods using Quickbird-2 and Landsat-8 imagery". Arabian journal of Geoscience, Springer, online, DOI:10.1007/s12517-017-2878-3.

- Jagalingam P and Arkal Vittal Hegde (2017). "A Comparative Study on Extraction of Buildings from Quickbird-2 Satellite Imagery with and without Fusion". Cogent Engineering, Taylor & Francis, 2017(4), 1-17.

5.5.2 Conference papers

- Jagalingam P and Arkal Vittal Hegde (2014). "Pixel Level Image Fusion - A Review on Various Techniques ". World Conference on Applied Sciences, Engineering and Technology, 3, 521-528, Kathmandu, Nepal. ISBN 13: 978-81-930222-0-7.

- Jagalingam P and Arkal Vittal Hegde (2015)."A Review of Quality Metrics for Fused Image". International Conference on Water Resources, Coastal And Ocean Engineering, Aquatic Procedia, Elsevier, 4, 133-142.

- Jagalingam P and Arkal Vittal Hegde (2015). "Bathymetry Mapping Using Landsat 8 Satellite Imagery". International Conference on Asian and Pacific coast (APAC 2015), 116, 560-566, Procedia Engineering, Elsevier.

- Jagalingam P and Arkal Vittal Hegde (2016). “Pan-sharpening the spatial resolution of LISS-IV image using a CARTOSAT-1 image”. 5th International Engineering Symposium (IES 2016), C3-5-1 to C3-5-6, Kumamoto university, Japan.

- Jagalingam P and Arkal Vittal Hegde (2016). “Improving the spatial resolution of multispectral imagery”. 10th International Symposium on Low land Technology (ISLT 2016), 342-346, In proceedings of 10th International Symposium on Low land Technology (ISLT 2016).

- Jagalingam P and Arkal Vittal Hegde (2017). “Building extraction from Quickbird-2 imagery”. 6th International Engineering Symposium (IES 2017), C1-6-1 to C1-6-5 , Kumamoto university, Japan.

BIO-DATA

JAGALINGAM P

Address for Correspondence

1/554, Hittakkal

Hittakkal post, Khotagiri, The Nilgiris, Tamilnadu, India - 643217.

E-mail: *lingam.jai10@gmail.com, am13f05@nitk.ac.in*

Mob: +91-8867824564

Academic Qualifications :

Master of Technology CGPA : 8.9

Adhiyamaan Engineering College, Hosur, Tamilnadu

Bachelor of Engineering Score : 71.6%

Anna University

Research Publications :

Articles in International Journals : 04

Articles in Journal Proceedings : 02

Papers presented in International Conferences : 04